Sensivitivity of Sea Surface Temperature over the Black Sea to Water Turbidity using HYCOM with the KPP mixed layer sub–model

A. Birol Kara, Alan J. Wallcraft and Harley E. Hurlburt

Naval Research Laboratory, Stennis Space Center, Mississippi

(submitted to *J. Phys. Oceanogr.* on July 31, 2003)

Corresponding author address: Birol Kara: Naval Research Laboratory, Code 7323, Bldg. 1009, Stennis Space Center, MS 39529–5004, USA.

E–mail: kara@nrlssc.navy.mil, wallcraft@nrlssc.navy.mil, and hurlburt@nrlssc.navy.mil

ABSTRACT

This paper examines the sensitivity of sea surface temperature (SST) to water turbidity in the Black Sea using the eddy–resolving HYbrid Coordinate Ocean Model (HYCOM) which includes a non–slab K–Profile Parameterization (KPP) mixed layer model. The KPP model uses a diffusive attenuation coefficient of Photosynthetically Available Radiation ($k_{\rm PAR}$) processed from a remotely–sensed data set to take water turbidity into account. Six model experiments (expt) are performed with no assimilation of any ocean data and wind/thermal forcing from two operational models: (1) European Centre for Medium–Range Weather Forecasts (ECMWF) re–analysis (ERA), and (2) Fleet Numerical Meteorology and Oceanography Center (FNMOC) Navy Operational Global Atmospheric Prediction System (NOGAPS). Forced with ECMWF, expt 1 uses spatially and monthly varying $k_{\rm PAR}$ values over the Black Sea, expt 2 assumes all of the solar radiation is absorbed at the sea surface, and expt 3 uses a constant $k_{\rm PAR}$ value of 0.06 $\rm m^{-1}$, representing clear water attenuation. The expts 4, 5 and 6 are twins of expts 1,2 and 3 but forced with the NOGAPS data. The monthly averaged model SSTs resulting from all experiments are then compared with a fine resolution satellite–based SST monthly climatology (the 1/8° Pathfinder climatology). Due to the high turbidity in the Black Sea, it is found that, a clear water constant attenuation depth (i.e., expts 3 and 6) results in SST bias as large as 3°C in comparison to standard simulations (expts 1 and 4) over most of the Black Sea in summer. In particular, when using the clear water constant attenuation depth as opposed to the using spatial and temporal $k_{\rm PAR}$, basin averaged SST RMS difference with respect to the Pathfinder SST climatology increases $\approx 46\%$ (from 1.41°C in expt 1 to 2.06°C in expt 3) in the ECMWF wind/thermal forcing case. Similarly, basin averaged SST RMS difference increases $\approx 36\%$ (from 1.39°C in expt 4 to 1.89°C in expt 6). The standard HYCOM simulations (expts 1 and 4) have a very high basin–averaged skill score of 0.95, showing overall model success in predicting climatological SST

even with no assimilation of any SST data. Relatively large model SST errors close to the coastal boundaries are attributed to the misrepresentation of land/sea mask in the ECMWF and NOGAPS products. Finally, it is shown that there is a linear relationship between SST differences and heat flux differences below the mixed layer. Specifically, a heat flux difference of ≈ 50 W m^{-2} sub–mixed layer heat flux results in a SST difference of $-\approx 3.0^{\circ}$C when using clear water constant attenuation depth as opposed to monthly varying $k_{\rm PAR}$ in the model simulations, clearly explaining potential impact of penetrating radiation on SST simulations.

1. Introduction and Motivation

The Black Sea is nearly land–locked, except for a narrow opening to the Bosporus Strait, and the ventilation of the deep waters by lateral influxes is therefore poor (Sur et al. 1996). Extensive biological activity in the Black Sea is evident from various studies (e.g., Konovalov and Murray 2001; Cokacar et al. 2001). The Black Sea also experiences large volumes of nutrients and contaminants from the Danube, Dniepr and Dniestr rivers along the northwestern shelf (e.g., Mee 1992). Permanent contamination due to the biological activities and river sources exists in the region because a strong density stratification effectively inhibits vertical mixing and ventilation of sub–pycnocline waters from the surface. Thus, prediction of upper ocean quantities in the region is closely tied to water turbidity in modeling studies.

Ocean General Circulation Models (OGCMs) with mixed layer sub–models are necessary to explain air—sea interactions and upper ocean characteristics, such as sea surface temperature (SST) whose prediction on a wide variety of temporal and spatial scales is the underlying goal of this paper. Realistic SST predictions from OGCMs are particularly needed over the biologically active Black Sea. For example, complex biogeochemical models include SST for constructing a mathematical framework in studying the ecosystem of the region (e.g., Oguz et al. 2002). In addition, given that the SST triggers the thermodynamic exchanges from ocean to

atmosphere, obtaining accurate SSTs from an OGCM becomes an important issue in the Black Sea, a region with many competing processes that are not accurately known, including air–sea exchange, oceanic transport, and vertical mixing.

In general, an OGCM needs to use the best available turbidity fields to predict SST (e.g., Murtugudde et al. 2002; Kara et al. 2003a). The reason is that the optical properties of the upper ocean can change the dynamical response of the mixed layer to atmospheric forcing, such as wind stress and heat fluxes. Not surprisingly, previous OGCM studies showed that SST is sensitive to the vertical distribution of the absorbed solar flux (e.g., Schneider and Zhu 1998; Rochford et al. 2001) due to the fact that the upper ocean is relatively transparent to solar radiation. In particular, $\approx 50\%$ of the sunlight penetrating the sea surface is composed of wavelengths longer than 780 nm (Morel and Maritorena 2001). The infrared radiation is absorbed and converted to heat near the ocean surface. Ultraviolet radiation has a wavelength of < 400 nm and forms only a small fraction of the total radiation (Lalli and Parsons 1997). The remaining 50% of the radiation comprises the visible spectrum with wavelengths between 400 nm and 700 nm that penetrate deeper to the ocean (e.g., Liu et al. 1994). These are approximately the same wavelengths used by plants in photosynthesis so these wavelengths are commonly referred to as Photosynthetically Active Radiation (PAR).

Given that the attenuation of PAR (k_{PAR}) is very large in all months, and mixed layer depth (MLD) is very shallow in the Black Sea, especially in summer (Kara et al., this issue), the sunlight penetration needs to be taken into account properly in an OGCM study. This requires the use of spatial and temporal varying turbidity fields. Thus, the Black Sea OGCM studies should use ocean turbidity at high spatial resolution as part of the heat flux forcing. This can be achieved by using remotely–sensed attenuation depths in the parameterization of solar subsurface heating. By doing so, the time–varying solar penetration schemes can then

treat attenuation as a continuous quantity, which is an improvement over the use of a few discrete attenuation values corresponding to classical Jerlov water types (Jerlov 1976). In fact, Kara et al. (this issue) also concluded that a single Jerlov water type could not be used for predicting stratification and surface currents in the Black Sea by demonstrating the impact of using a remotely–sensed attenuation depth climatology that is applicable to any OGCM that has fine vertical resolution near the surface.

Predicting SST at high spatial resolution also requires eddy–resolving OGCMs. However, there are only limited number of numerical ocean modeling studies for the Black Sea. Table 1 summarizes commonly used finer resolution OGCMs in the Black Sea. These models used various numbers of levels in vertical and varying grid resolutions. Most commonly used OGCMs in the Black Sea shown in Table 1 are earlier versions of the Princeton Ocean Model (POM) and the Modular Ocean Model (MOM). The POM is a free surface primitive equation ocean model for incompressible, Boussinessq and hydrostatic fluid (e.g., Blumberg and Mellor 1987). It employs bottom–following σ coordinate and coast-following orthogonal curvilinear coordinate systems, and includes the 2.5 turbulence closure scheme of (Mellor and Yamada 1982). The very early version of the MOM used in Black Sea model studies (e.g., Stanev et al. 1995; Stanev and Stenava 2000) is based on Bryan (1969). It is a z–coordinate OGCM. There are also a few other eddy–resolving OGCMs used in the Black Sea studies. For example, GeoHydrodynamics Environment Research (GHER) model is a primitive equation model (Nihoul et al. 1989; Beckers 1991), and the numerical resolution of the coupled set of non–linear partial differential equations is based on a vertical coordinate change (Deleersnijder and Beckers 1992). The Dietrich Center for Air Sea Technology (DieCAST) model is another OGCM used in the Black Sea by Staneva et al. (2001). It is a primitive equation, z-level, hydrostatic, fully conservative and Boussinessq ocean model (Dietrich 1997).

The main focus of the OGCM studies mentioned above (see also Table 1) was to examine directly/indirectly

dynamics of ocean circulation from different perspectives. In particular, upper ocean circulation including the Rim current system, interior cells involving various gyres and eddies were examined. These features are well–known characterictics of upper ocean circulation of the Black Sea (e.g., Sur et al. 1994; Besiktepe et al. 2001; Korotaev et al. 2001). However, none of these OGCM studies directly examined SST predictions in the Black Sea or gave any indication of the effect of water turbidity on the OGCM results. Because an examination of spatial and temporal SST variability is a neglected component of the Black Sea OGCM studies, we now investigate SST predictions from HYCOM. Such a hybrid coordinate model approach is optimal for the Black Sea because of the existence of a wide continental shelf. Using the layered continuity equation, HYCOM can make a dynamically smooth transition from isopycnal coordinates in the stratified ocean to a terrain–following coordinate in shallow coastal regions, and to z–level coordinates in the mixed layer and/or unstratified seas.

In this paper, our main purpose is three fold: (1) to demonstrate the capability of HYCOM to predict climatological SST on monthly time scales and discuss the effects of two different atmospheric forcing sets on the model simulations, (2) to examine effects of water turbidity on the SST simulations using a monthly mean attenuation depth climatology as constructed from a remotely–sensed data set, and (3) to perform extensive model–data comparisons using a set of statistical metrics along with evaluation criteria for sensitivity simulations. Accordingly, this paper is organized in the following manner. Section 2 briefly describes the OGCM (HYCOM) used in this paper along with its application to the Black Sea. Section 3 presents the model simulations and discusses the differences between net heat flux at the sea surface and the penetrating heat amount based on various water turbidity levels. Section 4 presents model–data comparisons and a brief description of statistical metrics. Section 5 investigates a possible linear relationship between heat flux differences and SST errors from the model. Finally, conclusions are given in section 6.

2. Ocean Model Description

The numerical ocean model used in this paper is based on a primitive–equation HYbrid Coordinate Ocean Model (HYCOM) as described in Bleck et al. (2002). HYCOM behaves like a conventional σ (terrain following) model in very shallow oceanic regions, like a z–level coordinate model in the mixed layer or other unstratified regions, and like an isopycnic–coordinate model in stratified regions. The model contains a total of five prognostic equations: two for the horizontal velocity components, a mass continuity or layer thickness tendency equation and two conservation equations for a pair of thermodynamic variables, such as salt and temperature or salt and density (see also Bleck et al. 2002). The main model additions we made towards the prediction of upper ocean quantities (especially for SST) are a new sea surface energy balance that accounts for spatial and temporal water turbidity and a new parameterization of longwave flux that has an effect on SST. Details of these new parameterizations are given in sections 2a, and 2b, respectively.

HYCOM uses a non–slab K–Profile Parameterization (KPP) mixed layer model (Large et al. 1994; 1997). The KPP is a 1st order turbulence closure ocean surface boundary layer model that is intermediate in computational complexity between bulk mixed layer models and 2nd order turbulence closures. It is currently the standard mixed layer sub–model for HYCOM because it is relatively insensitive to low vertical resolution, and the hybrid coordinate approach tends to require fewer layers/levels than fixed vertical coordinate approaches. The KPP scheme has primarily been tuned against Large Eddy Simulations (LES) and therefore typically over short time scales (e.g. the diurnal cycle) and in small regions. In this paper, the main interest is in longer time scales (monthly) over the Black Sea.

The KPP provides mixing from surface to bottom, matching the large surface boundary layer diffusivity/viscosity profiles to the weak diapycnal diffusivity/viscosity profiles of the interior ocean. There are

numerous advantages to this model. In the ocean interior, the contribution of background internal wave breaking, shear instability mixing, and double diffusion (both salt fingering and diffusive instability) are parameterized. In the surface boundary layer, the influences of wind–driven mixing, surface buoyancy fluxes, and convective instability are parameterized. The KPP algorithm parameterizes the influence of nonlocal mixing of temperature and salinity, which permits the development of countergradient fluxes. It is semi–implicit, requiring multiple iterations.

2a. Surface Energy Balance

Prior to executing the KPP algorithm, surface fluxes of thermodynamical variables and momentum are distributed entirely over the uppermost model layer, with the exception of penetrating shortwave radiation. Shortwave radiation can penetrate to deeper layers, with the penetration depth depending on water turbidity. The following contains a comparison of the previous HYCOM subsurface heating approach and the one used in this paper is provided.

Traditionally, the two–component (red and blue light) exponential decay model of Jerlov (1976) was used to calculate penetrating shortwave radiation in HYCOM. The depth of penetration was a function of water turbidity, represented by the Jerlov water type which was same everywhere in time and space. Given the incoming shortwave radiation flux S_0 at the surface, the flux passing through model interface k located at pressure p_k was expressed as follows:

$$S_k = S_0 \left[r \exp\left(\frac{-p_{k+1}}{\beta_R}\right) + (1-r) \exp\left(\frac{-p_{k+1}}{\beta_B}\right) \right], \tag{1}$$

where r is the fraction of light that is red, β_R is the penetration depth scale of red light, and β_B is the penetration depth scale of blue light. The r values for the classical Jerlov water types (Types I, IA, IB, II,

and III) are 0.58, 0.62, 0.67, 0.77 and 0.78%, respectively. The corresponding β_R values are 0.35, 0.60, 1.00, 1.50, and 1.40 m, and similarly, the β_B values are 23.0, 20.0, 17.0, 14.0, and 7.9 m, respectively.

In this paper, we use the satellite–based attenuation coefficients instead of a constant Jerlov value everywhere. With the new scheme introduced in Kara et al. (this issue), the net surface heat flux that has been absorbed (or lost) by the upper ocean to depth z, $Q(0)$, is parameterized as the sum of the downward surface solar irradiance ($Q_{\rm sol}$), upward longwave radiation ($Q_{\rm LW}$), and the downward latent and sensible heat fluxes (Q_L and Q_S, respectively).

$$Q(z) = (Q_{\rm sol}(0) - Q_{\rm sol}(z)) - Q_{\rm LW} + Q_L + Q_S, \quad (2)$$

$$Q_{\rm sol}(z)/Q_{\rm sol}(0) = (1-\gamma)\exp(-z/0.5) + \gamma\exp(-zk_{\rm PAR}), \quad (3)$$

$$\gamma = \max(0.27, 0.695 - 5.7k_{\rm PAR}), \quad (4)$$

Here $Q_{\rm sol}(z)$ is the amount of solar radiation that penetrates to depth. The rate of heating/cooling of the each layer is simply obtained by evaluating (2) at the bottom and top of the layer, with only $Q_{\rm sol}(z)$ non–zero below layer 1.

Latent and sensible heat fluxes at the air–sea interface are calculated using efficient and computationally inexpensive simple bulk formulae that include the effects of dynamic stability (Kara et al. 2002). The combination of accuracy and ease of computation of this method makes it the one preferred for computing air–sea fluxes in HYCOM. Note that both sensible and latent heat fluxes are calculated using top layer temperature at each model time step. Solar radiation flux (shortwave and longwave) is so dependent on cloudiness that this is taken directly from ECMWF (or NOGAPS) for use in the model. Basing fluxes on the model SST automatically provides a physically realistic tendency towards the correct SST. If the model SST is too high

or low, the flux is reduced or increased relative to that from the correct SST. The trend towards reality is typically sufficient on its own to keep the model SST approximately on track.

2b. Longwave Radiation Effects on SST

Blackbody longwave radiation into the ocean depends only on SST (T_s) as follows:

$$Q_{\rm bb} = -0.98\,\sigma\,(T_s + 273.16)^4, \tag{5}$$

where the Stefan–Boltzmann constant (σ) is 5.67×10^{-8}. There is a negative sign because this is heat lost from the ocean in HYCOM.

The net longwave flux is the sum of this upward blackbody term and the downward atmospheric longwave flux. It is dependent on cloudiness, and this is one reason why OGCMs, such as the Naval Research Laboratory Layered Ocean Model (NLOM) with an embedded mixed layer Wallcraft et al. (2003) and the Miami Isopycnic Coordinate Ocean Model (MICOM) as described in Bleck et al (1992), take the net longwave flux as an input atmospheric field. However, the blackbody flux is independent of cloudiness, and it is not clear that the downward atmospheric longwave flux is significantly dependent on SST (as opposed to the air temperature (T_a)). Common approximations of the net longwave flux assume that T_s, T_a and cloudiness are all related to the atmospheric longwave flux (e.g., Gupta et al. 1992), but the most recent mid to high latitude approximation (Josey et. al. 2003) suggests that the atmospheric longwave component depends on T_a and cloudiness alone.

If we assume that $Q_{\rm bb}$ is the only T_s dependent component of $Q_{\rm LW}$ and that it was calculated with a SST of $T_{\rm so}$, potentially different from the model SST of T_s,

$$Q_{\rm LW}(T_s) \;=\; Q_{\rm LW}(T_{\rm so}) + Q_{\rm bb}(T_s) - Q_{\rm bb}(T_{\rm so}), \tag{6}$$

$$Q_{\rm LW}(T_s) = Q_{\rm LW}(T_{\rm so}) + Q'_{\rm bb}(T_s)\,(T_s - T_{\rm so}), \tag{7}$$

$$Q'_{\rm bb} = -0.98\,\sigma\,4.0 * (T_s + 273.16)^3. \tag{8}$$

Here, it is noted that the parameterization in (7) is obtained by assuming $T_{\rm so} - T_s$ is small in (6). The cubic equation (8) is very well approximated in the range –2 to 32 by a linear fit (Figure 2) expressed as follows:

$$Q'_{\rm bb} \approx -4.506 - 0.0554\,T_s. \tag{9}$$

This gives -5.3 ± 0.8, so a constant value of –5.3 W m^{-2} C^{-1} is a fairly good approximation to the blackbody radiation correction. Overall, this is a much smaller effect than that of SST variations on latent and sensible heat fluxes, already allowed for by HYCOM; however, it is in the right direction (too warm a SST gives a negative longwave anomaly and to cool a positive anomaly).

For simulations using climatological atmospheric forcing, it is reasonable to assume that the climatological SST (T_c) was used to generate the longwave flux. The blackbody correction, can therefore be approximated as a relaxation term:

$$Q_{\rm LW}(T_s) = Q_{\rm LW}(T_c) - 5.3\,(T_s - T_c). \tag{10}$$

HYCOM already has such a term, expressed as an equivalent depth (H), for a 30 day e–folding time as follows:

$$Q_{\rm relax} = \frac{(H \times C_{\rm pw} \times \rho_0)}{(30 \times 86400)}(T_c - T_s), \tag{11}$$

where $C_{\rm pw}$ is specific heat of water (3990 J kg^{-1} K^{-1}) and ρ_0 is the water density (1000 kg m^{-3}). It is noted that based on (11), the H must be 3.5 m to get 5.3 W m^{-2} °C^{-1}. Similarly, the H must be 3 m to get 4.6 W m^{-2} °C^{-1}. This is a relatively small relaxation term well justified based on the need for a blackbody correction. All simulation presented in this paper used a H value of 3.5 m.

2c. Black Sea Model

The Black Sea model has a resolution of $1/25^\circ \times 1/25^\circ$ cos(lat), (longitude $\times$ latitude) ($\approx$ 3.2 km), which is at least 3 times finer than earlier OGCM studies shown in Table 1. There is a total of 15 hybrid layers in the model, and the target density (σ_t) values corresponding to layers 1 through 15 are 6.00, 9.00, 10.00, 11.00, 12.00, 12.80, 13.55, 14.30, 15.05, 16.20, 16.80, 16.95, 17.05, 17.15 and 17.20, respectively. The bottom topography in the model was constructed using various sources, including the 1 minute subregion of NAVOCEANO 's DBDB–V that covers the Mediterranean Sea including the Aegean Sea and Black Sea. It was first interpolated interpolated to the model grid; then, smoothed twice with a nine–point real smoother to reduce energy generation at small scales. The final bottom topography (see Kara et al. this issue) is used in the model simulations. The model is initialized using the temperature and salinity profiles from the Modular Ocean Data Assimilation System (MODAS) as described in (Fox et al. 2002). The climatology has a variable grid resolution: $1/8^\circ$ near land, $1/4^\circ$ over shallow shelves, and $1/2^\circ$ in the open ocean. Further details about the Black Sea model can be found in Kara et al. (this issue).

The climatological atmospheric forcing fields read in the model are wind stress and thermal forcing (air temperature, air mixing ratio, and net solar radiation). The model simulations presented in this paper use wind/thermal forcing from two different archived operational weather center products: (1) $1.125^\circ \times 1.125^\circ$ European Centre for Medium–Range Weather Forecasts (ECMWF) re–analysis product (Gibson et al. 1997) during 1979–1993, and (2) $1.0^\circ \times 1.0^\circ$ Fleet Numerical Meteorology and Oceanography Center (FNMOC) Navy Operational Global Atmospheric Prediction System (NOGAPS) data (Rosmond et al. 2002) during 1998–2002, separately. All model simulations are performed using climatological monthly mean forcing fields. However, a high frequency wind stress component is added to the climatological wind forcing because monthly winds do

not produce realistic MLDs (Wallcraft et al. 2003). The net surface heat flux in the model includes effects of turbidity through the model monthly $k_{\rm PAR}$ fields based on SeaWiFS (see section 2a).

The model treats rivers as a runoff addition to the surface precipitation field. The flow is first applied to a single ocean grid point and smoothed over surrounding ocean grid points, yielding a contribution to precipitation in m s^{-1}. In the Black Sea model, there are a total of six major rivers (Danube, Dniepr, Rioni, Dniestr, Sakarya and Kizilirmak) whose monthly mean climatological river discharge values were obtained from the readily available River DIScharge (RivDIS) data set (Vörösmarty et al. 1997). The Bosporus is considered a negative precipitation field to close the evaporation minus precipitation budget in the Black Sea. See Kara et al. (this issue) for a comparison of the climatological river discharge values in the Black Sea.

3. Model Simulations and Mixed Layer Flux

All HYCOM simulations are performed with no assimilation of any oceanic data except initialization to climatology and relaxation to sea surface salinity. The model is run until it reaches statistical equilibrium using climatological monthly mean thermal atmospheric forcing but wind forcing includes the 6–hourly variability. It takes about 5–8 model years for a simulation to reach the statistical equilibrium for all parameters.

Climatologically–forced model simulations that use three different $k_{\rm PAR}$ values were performed to investigate the effects of ocean turbidity for SST (Table 2). For expt 1 (the standard simulation), spatially and monthly varying $k_{\rm PAR}$ values interpolated to the HYCOM grid are used. For expt 2, all of the solar radiation is absorbed in the mixed layer by using a very large $k_{\rm PAR}$ value of 99.9 m^{-1}. For expt 3, the water turbidity over the Black Sea is set to a constant, $k_{\rm PAR} = 0.06$ m^{-1}, which is a representative value for clear water (e.g., Kara et al. 2003a,b). These experiments (i.e., expts 1, 2 and 3) use wind/thermal forcing from the ECMWF; while, expts 4, 5 and 6 are essentially twins of expts 1, 2 and 3 but use wind/thermal forcing from the NOGAPS,

respectively. In expt 3 an e–folding penetration depth of $k_{\rm PAR}^{-1}$ is 16.7 m. This is close to values used in recent OGCM studies: 17 m (Murtugudde et al. 2002), and 23 m (Nakamoto et al. 2001). Expt 2, which assumes all radiation absorbed at the sea surface, represents a traditional OGCM approach (e.g., Yuen et al. 1992).

Before an investigation is made on possible effects of water turbidity on the SST, we first calculate basin–wide mean heat flux at the sea surface. The mixed layer flux is the heat flux applied to the mixed layer in the model simulations. The difference between the basin–wide mean heat flux at the sea surface and mixed layer flux is shortwave radiation absorbed below the mixed layer. Figure 3 shows monthly means of total heat flux and mixed layer flux calculated from daily values. The monthly means were formed from the last 4 years of the model simulations during model years 5 through 8. Expts 2 and 5 assume all radiation at the sea surface so the basin–wide mean heat flux is equal to the mixed layer flux in these simulations. The basin–wide annual mean net heat flux at the sea surface is zero for all experiments because the Black Sea has closed boundaries so a model at equilibrium must have zero net surface flux.

The basin–wide annual mean values of heat flux below the mixed layer value are –17 and –40 W m^{-2} for expt 1 and expt 3, respectively. Similarly, they are –20 and –47 W m^{-2} for expt 4 and expt 6, respectively. Thus, the clear water constant attenuation depth assumption (i.e., expts 3 and 6) results in a larger net flux below the mixed layer over the Black Sea. Large shortwave radiation absorbed below the mixed layer are only seen in spring and summer. The largest difference between the net heat flux at the sea surface and the heat flux in th mixed layer is in June. In particular, the differences (i.e., the shortwave radiation below the mixed layer) in June are 40, 86, 44 and 97 W m^{-2} for expts 1, 3, 4 and 6, respectively.

4. HYCOM–Data Comparisons

In this section, several statistical metrics are used to inter–compare monthly mean SSTs obtained from

the climatologically–forced HYCOM simulations (expts 1 through 6) and to compare them with a satellite–based climatological SST data set. These comparisons are designed to examine the sensitivity of model SST to water turbidity. For evaluation of the model results, monthly mean SSTs are formed from daily fields using the last 4 model years (years 5 through 8). These values are then compared to climatology at each grid point of the Black Sea. At least a 4–year mean was needed because HYCOM with 3.2 km resolution has a strong nondeterministic component due to flow instabilities. These are a major contribution to the simulated Black Sea circulation at this resolution.

Given that all forcing in HYCOM simulations is climatological, monthly mean HYCOM SSTs can be compared with climatological monthly mean SSTs. The climatological SST used in this paper is the Pathfinder data set (Casey and Cornillon 1999) which is based directly on satellite data during 1985–1997. The annual Pathfinder SST climatology interpolated to the HYCOM domain is shown in Figure 4a. It has a resolution of 9.28 km ($\approx 1/8^\circ$). The climatology is created by averaging daily fields into monthly time series. Both daytime and nighttime daily fields are included in each monthly average. A 7×7 median filter is applied to fill in many of the gaps, and a 7×7 median smoother is used for entire field to remove small–scale noise, The Pathfinder climatology is preferred for the HYCOM model–comparisons for two main reasons: (1) as explained in Casey and Cornillon (1999), the Pathfinder climatology outperforms the commonly used climatologies, such as the $1^\circ \times 1^\circ$ U.K. Meterological Office Global Ice and Sea Surface Temperature (GISST) climatology (Rayner et al. 1996), the $1^\circ \times 1^\circ$ World Ocean Atlas 1994 (WOA94) climatology (Levitus and Boyer 1994) which does not include the Black Sea at all and the $1^\circ \times 1^\circ$ National Oceanic and Atmospheric Administration (NOAA) Optimal Interpolation (OI) SST climatology (Smith and Reynolds 1998), shown in Figure 4b, and (2) it has much finer resolution ($1/8^\circ$) than the others, which is the appropriate for the fine resolution Black Sea model

used in this paper.

To validate HYCOM SST there are also other observed climatological data sources that can be used, such as the later version of the NOAA optimal interpolation SST climatology (Reynolds et al. 2002) and the Comprehensive Ocean Atmosphere Data Set (COADS) SST climatology (da Silva et al. 1994). However, they are still on the $1^\circ \times 1^\circ$ grid. Even though the MODAS climatology as described in section 2c has a fine resolution to validate model results, it is a bi–monthly data set and was already used in the model initilization. Thus, it is not used for the model–data comparisons.

Here it is noted that annual mean SST biases between the Pathfinder climatology and NOAA OI climatology are not larger than 0.5°C in most of the region except the northwestern shelf where there was an annual mean bias up to 2°C (Figure 4). However, there are differences in air temperatures at 10 m above the sea surface between ECMWF and NOGAPS which are used in the model simulations as part of the thermal forcing.

4a. Statistical Metrics

Different statistical measures are considered together to measure the strength of the relationship between SST values predicted by the model (HYCOM SST) and those from the climatology (Pathfinder SST). The latter is interpolated to the model grid for model–data comparisons. We evaluate time series of monthly mean SST at each model grid point over the Black Sea. Following Murphy (1988), the statistical relationships used here between the 12 monthly mean Pathfinder SST (X) and HYCOM SST (Y) can be expressed as follows:

$$\mathrm{ME} = \overline{Y} - \overline{X}, \tag{12}$$

$$\mathrm{RMS} = \left[\frac{1}{n}\sum_{i=1}^{n}(Y_i - X_i)^2\right]^{1/2}, \tag{13}$$

$$R = \frac{1}{n}\sum_{i=1}^{n}(X_i - \overline{X})(Y_i - \overline{Y}) / (\sigma_X \sigma_Y), \tag{14}$$

$$\mathrm{SS} = R^2 - \underbrace{[R - (\sigma_Y/\sigma_X)]^2}_{B_{\mathrm{cond}}} - \underbrace{[(\overline{Y} - \overline{X})/\sigma_X]^2}_{B_{\mathrm{uncond}}}, \tag{15}$$

where $n = 12$, ME is the mean error, RMS is the root–mean–square difference, R is the correlation coefficient, SS is the skill score, and $\overline{X}$ ($\overline{Y}$) and σ_X (σ_Y) are the mean and standard deviations of the Pathfinder (HYCOM) SST values, respectively. For the 12 monthly SST fields at each grid point over the Black Sea, the R value between HYCOM and Pathfinder SST must be at least ± 0.53 for it to be statistically different from a R value of zero based on the student's t–test at the 95% confidence interval (Neter et al. 1988).

The nondimensional SS is given in (15), and it includes conditional and unconditional biases (Murphy 1992). It is used for the model–data comparisons because one needs to examine more than the shape of the seasonal cycle using R. The non–dimensional SS measures the accuracy of SST simulations relative to Pathfinder SST. The conditional bias (B_{cond}) is the bias in standard deviation of the HYCOM SST, while the unconditional bias (B_{uncond}) is the mismatch between the mean HYCOM and Pathfinder SST. A simple definition for SS, based on RMS difference, is $\mathrm{SS} = 1 - \mathrm{RMS}^2/\sigma_X^2$ as given in Murphy and Daan (1985). The value of R^2 can be considered a measure of "potential" skill, i.e., the skill that one can obtain by eliminating bias from the HYCOM SST. Note the SS is 1.0 for perfect HYCOM SSTs. The nondimensional SS takes bias into account, something not done by R. Part of the reduction in SS values in comparison to R stems from the squaring of correlation in the SS calculation. Biases are taken into account in the RMS differences, but the latter can be small where SS and R are poor because the amplitude of seasonal cycle might be small at some locations.

4b. SST predictions from HYCOM

Sensitivity of HYCOM to water turbidity is first examined using annual bias (i.e., mean error, ME) maps between the HYCOM simulations. Annual mean SST from each experiment is formed (Figure 5a), and the departure of HYCOM SST from the climatological 1/8° Pathfinder SST (Figure 5b) is calculated. Overall, the SST errors in the interior are usually smaller than those along continental boundaries, and the ME for the standard simulations (i.e., expts 1 and 4) that use SeaWiFS–based spatial and temporal varying attenuation depths is usually less than ±0.5°C in the interior of the Black Sea. In fact, the basin averaged annual ME values are –0.54°, –0.49°, and –0.85°C for expts 1,2 and 3, respectively. Similarly, they are 0.19°, 0.25°, and –0.07°C for expts 4,5 and 6, respectively. While the ME is small in expt 6 which assumes clear water constant attenuation depth, we will later show that RMS difference and (1–SS) values are relatively large, clearly indicating the importance of using various statistical metrics in deciding which experiment performed the best.

As to individual monthly mean analysis, Figure 6a shows ME values in February. In comparison to standard experiments (i.e., expt 1 and 4), it is clear that absorbing all radiation at the sea surface results in a negligible cold bias, and this is true when using both ECMWF wind/thermal forcing and NOGAPS wind/thermal forcing. In other words, SSTs from expts 2 and 5 are slightly colder than those from expts 1 and 4. Overall, the mean SST bias is between –0.25° and 0.25°C over the most of the Black Sea as this is also evident from the basin averaged SST differences values given in Table 3. On the other hand, the clear water assumption (i.e., expts 3 and 6) yields significantly warmer February SSTs in comparison to the standard simulations (see Figure 6a).

When HYCOM SST from the standard simulation is compared to the Pathfinder SST climatology, the model usually gives a warm bias. In comparison Pathfinder the HYCOM SST prediction in the northwestern

shelf shows significant differences in accuracy depending on the atmospheric forcing product. While there is almost no bias (or a slightly warm bias) in the NOGAPS wind/thermal forcing case, a significantly large cold SST bias is evident in the ECMWF wind/thermal forcing case, indicating an effect of the atmospheric forcing product on the model simulations. The big difference in SST is attributed to the amount of solar radiation being different in the two products. As evident from spatial plots of shortwave radiation (see Kara et al. this issue), the annual mean difference between ECMWF and NOGAPS can be as large as 70 W m^{-2} in the northwestern shelf.

Effects of water turbidity on the SST predictions from HYCOM are especially evident in June when there can be differences as large as 3°C (Figure 6b). The assumption of all radiation at the sea surface results in a systematic warm bias over the Black Sea in comparison to the standard experiments. However, compared to expts 2 and 5, there are much larger SST differences when using a constant clear water attenuation depth ($\approx$ 17 m) in the model simulations (i.e., expts 3 and 6) as seen from (Figure 6b), and unlike February there is a cold bias in June. In particular the basin averaged SST difference (see Table 3) between expt 3 and expt 1 (expt 6 and expt 4) is –2.1°C (–1.7°C). Obviously, very shallow summer MLD is the main reason of seeing these large SST differences. For example, basin averaged mean MLD values in February are 43 and 46 m for expts 3 and 6, respectively; while, basin averaged mean MLD values in June are only 4.1 and 4.6 m, respectively. The latter values are more than 4 times shallower than the constant clear water attenuation depth assumption of $\approx$ 16.7 m as used in expts 3 and 6. Note that based on the optimal layer depth definition of Kara et al (2000), the Black Sea has MLDs as shallow as 3 m in summer (not shown here). This is much shallower than in most other regions of the global ocean (Kara et al. 2003c).

HYCOM skill in reproducing the climatological SST is now evaluated in terms of RMS difference and SS.

For this purpose, the monthly mean Pathfinder SST climatology is taken as a reference data set and compared to the monthly HYCOM SST. This is done for each experiment. Figure 7 shows RMS differences computed on model grid over the Black Sea. It shows that expts 1 and 2 give relatively small RMS differences. As we calculated, the standard deviation of SST is usually $> 5°$C for the annual cycle, confirming that there is strong seasonal SST variability in the Black Sea. Thus, the RMS difference values in expt 1 (≈ 1 °C) are much smaller. This is especially evident in the interior of the Black Sea. Large RMS differences are seen in expt 3 which uses a clear water constant attenuation depth assumption. In this case, RMS differences as large as 3°C are noted along continental boundaries in the eastern part of the Black Sea. However, some of the errors close to the coastal regions are due to land–sea mask used in atmospheric forcing products as will be explained in section 4c.

When using the NOGAPS wind/thermal forcing (i.e., expts 4,5 and 6), SST RMS differences are similar to the ones using the ECMWF wind/thermal forcing. The standard simulation (expt 4) has slightly larger RMS values than expt 1 because there is more subsurface heating in the NOGAPS wind/thermal forcing simulations due to relatively large shortwave radiation (see Figure 3). In general, there are not large RMS differences when using the monthly varying attenuation depths as opposed to the simulation which assumes all radiation absorbed at the sea surface (expt 5); although, changes in SST can be 1° or 2°C in summer months, e.g, in June in these cases (see Figure 6b). This is also true for both ECMWF wind/thermal forcing cases (i.e., expt 1 vs expt 2). Similar to the expt 3, the clear water constant attenuation depth assumption in expt 6 also results in the largest RMS differences with respect to Pathfinder SST climatology. Another interesting feature of the RMS difference maps is that there is very small SST RMS difference ($< 1°$C) in the northwestern shelf when using the NOGAPS wind/thermal forcing; while, the RMS values are usually large ($> 2°$C) in the same

region when using ECMWF wind/thermal forcing (see section 4c for further explanation).

HYCOM success in predicting SST is especially evident from the SS map with values being close to 1 in the standard simulations (expts 1 and 4) over most of the Black Sea (Figure 7b). The basin–averaged SST standard deviation is as large as 6.4°C in the Black Sea during the 12–month period. By reproducing this variability, HYCOM is able to simulate the SST seasonal cycle remarkably well. The assumption of all radiation absorbed at the surface (expts 2 and 5) as opposed to the standard cases using variable attenuations depths did not significantly affect the SS. In contrast, SS values obtained from the simulations which use the clear water constant constant attenuation depths (expts 3 and 6) are relatively low in comparison to the standard simulations. Similar to the RMS difference map (see Figure 7a), the most obvious feature of the SS maps is that the water turbidity does not have any effect in the northwestern shelf where the water turbidity is already very high (expts 1 and 4 vs expts 2 and 5). The use of NOGAPS wind/thermal forcing in the model simulations results in the best SST prediction in this region. In fact, the largest SS values in expt 4 (see Figure 7b) are seen in the northwestern shelf north of $\approx 45°$N; while, the smallest SS values in expt 1 are evident at this region. Note that SS is never negative in any of the experiments, and the lowest SS value (0.48) is seen in expt 3. Any positive SS value is considered as representative of a successful prediction.

Finally, basin averaged SST error statistics (Table 4) summarize results for each experiment. When using monthly varying attenuation depth rather than constant attenuation depth, the HYCOM performance in predicting SST increases significantly. In the case of ECMWF wind/thermal forcing, the basin averaged RMS difference increases $\approx 46\%$, from 1.41°C (expt 1) to 2.06°C (expt 3). Similarly, In the case of NOGAPS wind/thermal forcing the basin averaged RMS difference increases $\approx 36\%$, from 1.39°C (expt 4) to 1.89°C (expt 6). It is noted that although the basin averaged annual mean SST bias is small between the two

experiments (e.g., expt 1 vs expt 3 and expt 4 vs expt 6), there are large biases up to 3°C in some individual months. In winter, the mean errors (i.e., expt 3–expt 1 and expt 6–expt 4) are usually positive (warmer winter SST when Black Sea turbidity is neglected); while, in summer mean difference is usually negative. Thus, the clear water assumption gives fairly small annual mean error with the winter warm bias and the summer cool bias tending to cancel each other out.

It should be noted that based on results from a layered ocean model (NLOM) with an embedded mixed layer (Kara et al. 2003a), it was found that the standard spatial and temporal varying k_{PAR} simulation was closer to the clear water constant attenuation depth case (k_{PAR}=0.06 m^{-1}) because the global ocean is not very turbid on average and because globally NLOM's mixed layer was relatively deep (including a 10 m minimum). However, in some regions global NLOM results were reasonable with all the radiation absorbed in the mixed layer. In the Black Sea, the standard experiments which use space/time variation in attenuation depths (expts 1 and 4) are much closer to the experiments which assume all radiation absorbed at the surface (expts 2 and 5, respectively) because of its high turbidity. Thus, an OGCM will need to use a spatially varying turbidity.

4c. Limitations in the Atmospheric Forcing

The grid resolution from the operational weather products ($1.125^\circ \times 1.125^\circ$ for ECMWF and $1.0^\circ \times 1.0^\circ$ for NOGAPS) is much coarser than the HYCOM grid resolution used here ($1/25^\circ \times 1/32^\circ$), and some atmospheric surface forcing fields are strongly influenced by land and sea. Thus, the land/sea mask used by these operational models is important, especially for regions close to the coast in the Black Sea. Given the fact that the SST errors from the standard HYCOM simulations (expts 1 and 4) as discussed in section 4b were very large in comparison to the Pathfinder climatology especially in the northern coast and eastern most Black Sea, we

now examine if these errors can be attributed to a possible misrepresentation of ocean points in the forcing products.

The land/sea masks used in the original ECMWF re–analysis and NOGAPS products interpolated onto the HYCOM domain are shown in Figure 9. Regarding the ECMWF land/sea mask, it is obvious that all points are on land south 41.2°N but most of them should be on ocean. There is only one sea grid point east of 39°E in the north–south direction, but there should be 2–3 grid points, in reality. It is also clear that ECMWF land–sea mask has one grid point over ocean at $\approx$ (31.2°E, 46°N), and three sea grid points below this at $\approx$ 45°N. This means that ECMWF assumes some points are over land or may have problems representing sea points near land in the HYCOM simulations. The NOGAPS mask provides a better representation of the land/sea distribution, but is still limited by its $1.0° \times 1.0°$ resolution. The fact that NOGAPS forcing shows more skill near the coast, despite generally lower skill elsewhere suggests that SST errors close to the coast, especially in the easternmost parts of the Black Sea, are primarily caused by the incorrect land/sea masks and not by HYCOM itself.

5. Flux and SST Relationship

To further investigate sensitivity of HYCOM SST simulations to water turbidity, a possible relationship between heat fluxes and SST is sought. Our major goals are (1) to determine if changes in heat fluxes cause systematic biases in SST, and if there are systematic biases, then (2) to find out the statistical relationship between the SST biases and heat flux biases. For this purpose, basin–averaged monthly mean net heat flux at the sea surface and mixed layer flux as introduced in section 3 (see Figure 3) are used along with monthly mean SST differences (see Table 3). As a first step, the heat flux difference below the mixed layer between the two simulations (e.g., between expt 1 and expt 3) is calculated. In other words, by using the difference

values between net heat flux at the sea surface and heat flux applied to the mixed layer from expt 1 and expt 3, another difference in flux values between the two simulations (i.e., expt 3–expt 1) is formed. Then, these flux differences are plotted against monthly mean SST differences for the same experiment pairs (i.e., expt 3–expt 1). Note that SST differences are already given in Table 3. The similar procedure is also applied to other experiment pairs.

Climatological monthly mean flux and SST differences averaged over the Black Sea (Figure 10) clearly suggest that there is an inverse linear relationship between the two. This confirms our first goal (1) above because changes in the heat flux differences are proportional to changes in SST differences. In other words, when the heat flux differences increase/decrease, SST differences decrease/increase. This is true for expt 3–expt 1 and expt 2–expt 1 which use ECMWF wind/thermal forcing. Similarly, the same is true for expt 6–expt 4 and expt 6–expt 5 which use NOGAPS wind/thermal forcing. Thus, there are two main conclusions from Figure 10. The first conclusion is that the flux differences are strongly related to SST differences when using clear water constant attenuation depth (i.e., expts. 3 and 6) or assuming all radiation absorbed at the sea surface (expts 2 and 4) in comparison to the standard simulations (i.e., expts 1 and 4). The second conclusion is that such a relationship exists for both ECMWF and NOGAPS forcing products, implying that model SST differences are dependent of heat flux differences regardless of the atmospheric forcing product.

We now seek a possible linear relationship (as suggested by Figure 10) between the SST differences and heat flux differences to attain the second goal. While it is clear that HYCOM SST is determined by various dynamical factors, the major focus here is only changes in heat fluxes and their possible effects on SST. Thus, it is assumed that SST differences are mainly controlled by heat fux differences between the experiment pairs (e.g., between expt 1 and expt 3). This means, for simplicity, it is assumed that SST difference is only a

function of the heat flux difference. A scatter diagram (Figure 11) indicates that SST differences are linearly correlated to heat flux differences with very large R values of 0.97 for both expt 3–expt 1 and expt 6–expt 4. These R values are statistically significant in comparison to a R value of 0.7 at 95% confidence interval.

The least squares lines for expt 3–expt 1 and expt 6–expt 4 have slope values of –0.065°C/W m^{-2} and –0.058°C/W m^{-2}, respectively. Based on the slope values, for example, a flux difference of 30 W m^{-2} between expt 3 and expt 1 results in a SST difference of $-\approx$ 1.9°C between the two. Similarly, a 50 W m^{-2} flux difference causes a SST difference which can be as large as $-\approx$ 3.3°C between expt 3 and expt 1. Thus, the assumption of clear water all over the Black Sea yields very unrealistic SST from the model (expt 3) in comparison to the standard simulation (expt 1). The same analogy can also be made between expt 6 and expt 4. Given that the slope value is –0.058°C/W m^{-2} between expt 6 and expt 4, heat flux differences of 30 and 50 W m^{-2} result in SST differences of $\approx$ –1.7 and –2.9°C between the two, respectively.

A similar investigation is also made to see whether or not there is any linear relationship between the simulations which assume all radiation absorbed at the sea surface (expts 2 and 5) and standard simulations (expts 1 and 4). Linear relationships are again quite remarkable as evident from statistically significant R values of 0.95 and 0.98 for expt 2–expt 1 and expt 5–expt 4, respectively. Slopes of the least squares lines for expt 2–expt 1 and expt 5–expt 4 are almost equal to each other with values of –0.020°C/W m^{-2} and –0.019°C/W m^{-2}, respectively. Thus, a flux difference of, for example, 50 W m^{-2} between expt 2 and expt 1 (or between expt 5 and expt 4) gives a SST difference of $-\approx$ 1.0°C. Therefore, there are indeed changes in SST in the HYCOM simulations which assume all radiation absorbed at the sea surface as opposed to the ones which use spatial and temporal monthly mean attenuation depths.

6. Summary and Conclusions

Ocean general Circulation Models (OGCMs) play an important role in representing the ocean component of the climate system on a wide variety of temporal and spatial scales. This paper shows that a fine resolution ($\approx$ 3.2 km) eddy–resolving HYbrid Coordinate Ocean Model (HYCOM) is particularly useful for simulating sea surface temperature (SST) and examining SST sensitivity to water turbidity in the Black Sea. This model combines the advantages of the isopycnal, σ and z–level coordinates in optimally simulating coastal and open–ocean circulation features, which does not exist in previous Black Sea OGCM studies. HYCOM includes the K–Profile Parameterization (KPP) mixed layer sub–model. The implementation of the KPP model used here has a two–band solar radiation penetration scheme which uses a monthly diffusive attenuation coefficient of Photosynthetically Available Radiation ($k_{\rm PAR}$) climatology to take water turbidity into account.

In the model simulations presented in this paper, the basic methodology is to force the model with monthly climatological atmospheric fields (i.e., wind and thermal forcing) from two operational weather prediction models, but with the addition of representative 6–hourly wind stress anomalies, using the model SST and an accurate bulk formula to calculate latent and sensible heat fluxes. A longwave radiation correction is used in the model simulations. The idea is that we have a longwave radiation field from an operational weather product used in forcing the model (e.g., from ECMWF) but that field was calculated using a different SST. Thus, we need a correction. It is found that a constant value of –5.3 W m^{-2} C^{-1} is a fairly good approximation to the blackbody radiation correction. Such an approach, as presented in this paper, is also applicable to other OGCMs. The model is initialized using temperature and salinity from a fine resolution Modular Ocean Data Assimilation System (MODAS) climatology. There is a weak sea surface salinity relaxation to bi–monthly MODAS but there is no relaxation to observed SST and no other ocean data assimilation.

Model simulations are performed to examine effects of water turbidity in predicting SST. For a quantita-

tive evaluation of the model performance, several statistical measures, such as mean error (ME), root–mean–square (RMS) difference, correlation coefficient (R), and skill score (SS) are used. Time series of monthly mean SST from HYCOM are then compared to those from a satellite–based climatological field (1/8° Pathfinder SST climatology) at each model grid point over the Black Sea . Climatological error statistics from standard HYCOM simulations, which use spatial and temporal attenuation depths, show that the model gives a basin–averaged ME of $-\approx 0.5$°C and RMS difference of 1.4°C for the seasonal cycle of SST. Similarly, basin averaged R and SS values are ≈ 0.95 and ≈ 0.99, respectively. Given that SST standard deviation is very large (usually > 5°C) over the Black Sea, having a very large SS value close to 1 clearly demonstrates HYCOM success in predicting monthly mean SST.

Further model–data comparisons reveal that while allowing k_{PAR} to vary in time and space is desirable for predicting SST in the Black Sea, absorption of all radiation at the sea surface also yields comparable results. In contrast, using the clear water constant attenuation depth assumption of $k_{\mathrm{PAR}} = 0.06$ m^{-1} (i.e., $k_{\mathrm{PAR}}^{-1} \approx 16.7$ m as opposed to using monthly–varying water type results in the worst SST simulation from the model over the Black Sea. In this case, the basin averaged SST bias values between the two simulations are found to be as large as 2°– 3°C in the summer. This large bias is due mainly to differences in the amount of heat flux below the mixed layer in the two cases. In particular, the simulation which assumes clear water constant attenuation depth over the Black Sea results in large sub–mixed layer heat flux difference compared to the standard simulation which uses spatial and temporal attenuation depths. In the latter, the attenuation depths are much smaller than 16.7 m. Thus, it is concluded the combination of relatively small attenuation depths along with the shallow mixed layer depths is the main reason of seeing these large flux and SST differences in summer. We also showed that SST differences and heat flux differences between the two simulations which

use various k_{PAR} values are linearly correlated to each other on seasonal climatological time scales.

Finally, the ability of HYCOM to predict SST in some regions may be limited by the atmospheric forcing product used. In particular, some of model errors near coastal regions (especially in the eastern Black Sea) are probably due to the land/sea mask used and the relatively coarse resolution of atmospheric forcing products. Results presented in this paper confirm accuracy of the model. Thus, the model simulation can be extended on interannual time scales, which is the subject of another paper.

Acknowledgments

We would like to extend our special thanks to E. J. Metzger and P. Posey of the Naval Research Laboratory (NRL) at the Stennis Space Center for their suggestions regarding atmospheric forcing fields. Appreciation is extended to R. Bleck of the Los Alamos National Laboratory (LANL), E. Chassignet and G. Halliwell of the Rosenstiel School of Marine & Atmospheric Science (RSMAS) at the University of Miami for their discusions during the HYCOM development. P. Kållberg of the European Centre for Medium–Range Weather Forecasts (ECMWF) is thanked his comments regarding the land/sea mask. The ocean color data used in this paper were obtained from the Goddard Distributed Active Archive Center under the auspices of the National Aeronautics and Space Administration (NASA). Use of this data is in accord with the Sea–viewing Wide Field–of–view Sensor (SeaWiFS) Research Data Use Terms and Conditions Agreement. The model simulations were performed under the Department of Defense High Performance Computing Modernization Program on a IBM SP POWER3 at the Naval Oceanographic Office, Stennis Space Center, Mississippi and on a HP/COMPAQ SC45 at the United States Army Engineer Research and Development Center (ERDC), Vicksburg, Mississippi. This work is a contribution of the 6.2 HYbrid Coordinate Ocean Model and advanced data assimilation, and the 6.1 Thermodynamic and Topographic Forcing of Global Ocean Models project. Both

are funded by the Office of Naval Research (ONR) under program elements 602435N for 6.2 and 601153N for 6.1 projects. This is contribution NRL/JA/7320/03/0019 and has been approved for public release.

References

Beckers, J.–M., 1991: Application of a 3D model to the Western Mediterranean. *J. Mar. Sys.*, **1**, 315–332.

Besiktepe, S. T., C. J. Lozano, and A. R. Robinson, 2001: On the summer mesoscale variability of the Black Sea. *J. Mar. Sys.*, **59**, 475–515.

Bleck, R., 2002: An oceanic general circulation model framed in hybrid isopycnic–cartesian coordinates. *Ocean Modelling*, **4**, 55–88.

——, C. Rooth, D. Hu, and L. Smith, 1992: Salinity–driven thermocline transients in a wind– and thermohaline–forced isopycnic coordinate model of the North Atlantic. *J. Phys. Oceanogr.*, **22**, 1486–1505.

Blumberg, A. F., and G. L. Mellor, 1987: A description of a three dimensional coastal ocean model. *Three Dimensional Shelf Models Coastal Estuarine Sci.*, Vol. 5, Heaps, N., Ed., 1–16.

Bryan, K., 1969: A numerical method for the study of the circulation of the world ocean. *J. Comp. Physics*, **3**, 347–378.

Casey, K. S., and P. Cornillon, 1999: A comparison of satellite and in situ based sea surface temperature climatologies. *J. Climate*, **12**, 1848–1863.

Cokacar, T., N. Kubilay, and T. Oguz, 2001: Structure of *Emiliania huxleyi* blooms in the Black Sea surface waters as detected by SeaWiFS Imagery. *Geophys. Res. Lett.*, **28**, 4607–4610.

da Silva, A. M., C. C. Young, and S. Levitus, 1994: *Atlas of Surface Marine Data.* Vol. 1: *Algorithms and Procedures.* NOAA Atlas NESDIS 6, U.S. Dept. of Commerce, Washington, D.C., 83 pp.

Deleersnijder, E., and J.–M. Beckers, 1992: On the use of σ–coordinate system in regions of large bathymetric

variations. *J. Mar. Sys.*, **3**, 381–390.

Dietrich, D. E., 1997: Application of a modified "a" grid ocean model having reduced numerical dispersion to the Gulf of Mexico circulation. *Dyn. Atmos. Oceans*, **27**, 201–217.

Fox, D. N., W. J. Teague, C. N. Barron, M. R. Carnes, and C. M. Lee, 2002: The Modular Ocean Data Assimilation System (MODAS). *J. Atmos. Oceanic Technol.*, **19**, 240–252.

Gibson, J. K., P. Kållberg, S. Uppala, A. Hernandez, A. Nomura, and E. Serrano, 1997: ERA description. ECMWF Re–Analysis Project Report Series, No. 1, 72 pp. [Available from ECMWF, Shinfield Park, Reading RG2 9AX, UK.]

Gupta, S. K., W. L. Darnell, and A. C. Wilber, 1992: A parameterization for longwave radiation from satellite data: Recent improvements. *J. Appl. Meteor.*, **31**, 1361–1367.

Jerlov, N. G., 1976: *Marine Optics. Elseiver Ocean. Ser.*, **14**, Elseiver, New York, 231 pp.

Josey, S. A., R. W. Pascal, P. K. Taylor, and M. J. Yelland, 2003: A new formula for determining the atmospheric longwave flux at the ocean surface at mid–high latitudes. *J. Geophys. Res.*, **108**, 3108, doi:10.1029/2002JC001418.

Kara, A. B., A. J. Wallcraft, and H. E. Hurlburt, 2003: A fine resolution HYbrid Coordinate Ocean Model (HYCOM) for the Black Sea with a new solar radiation penetration scheme: The impact of subsurface heating and attenuation depths on the surface circulation. *J. Phys. Oceanogr.*, submitted for the same issue.

——, H. E. Hurlburt, P. A. Rochford, and J. J. O'Brien, 2003a: The impact of water turbidity on the interannual sea surface temperature simulations in a layered global ocean model. *J. Phys. Oceanogr.*, in review.

——, ——, and P. A. Rochford, 2003b: Compensation depth and its relation to solar radiation attenuation

over the global ocean. *J. Phys. Oceanogr.*, in review.

Kara, A. B., P. A. Rochford, and H. E. Hurlburt, 2003c: Mixed layer depth variability over the global ocean. *J. Geophys. Res.*, **108**, 3079, doi:10.1029/2000JC000736.

——, P. A. Rochford, and H. E. Hurlburt, 2002: Air–sea flux estimates and the 1997–1998 ENSO event. *Bound.–Layer Meteor.*, **103**, 439–458.

——, ——, and ——, 2000: An optimal definition for ocean mixed layer depth. *J. Geophys. Res.*, **105**, 16 803–16 821.

Konovalov, S. K., and J. W. Murray, 2001: Variations in the chemistry of the Black Sea on a time scale of decades (1960–1995). *J. Mar. Sys.*, **31**, 217–243.

Korotaev, G. K., O. A. Saenko, and C. J. Koblinsky, 2001: Satellite altimeter observations of the Black Sea. *J. Geophys. Res.*, **106**, 917–933.

Kourafalou, V. H., and E. V. Stanev, 2001: Modeling the impact of atmospheric and terrestrial inputs on the Black Sea coastal dynamics. *Ann. Geophysicae*, **19**, 245–256.

Lalli, C. M., and T. R. Parsons, 1997: *Biological Oceanography: An Introduction.* Butterworth–Heinemann, Woburn, Mass., 314 pp.

Large, W. G., G. Danabasoglu, S. C. Doney, and J. C. McWilliams, 1997: Sensitivity to surface forcing and boundary layer mixing in a global ocean model: Annual mean climatology. *J. Phys. Oceanogr.*, **27**, 2418–2447.

——, J. C. McWilliams, and S. C. Doney, 1994: Oceanic vertical mixing: A review and a model with a nonlocal boundary layer parameterization. *Rev. Geophys.*, **32**, 363–403.

Levitus, S., and T. P. Boyer, 1994: *World Ocean Atlas 1994.* Vol. 4: *Temperature. NOAA Atlas NESDIS 4*,

U.S. Govt. Printing Office, Washington, D.C., 117 pp.

Liu, W. T., A. Zhang, and J. K. B. Bishop, 1994: Evaporation and solar irradiance as regulators of sea surface temperature in annual and interannual changes. *J. Geophys. Res.*, **99**, 12 623–12 637.

Mee, L. D., 1992: The Black Sea in crisis: A need for concerted international action. *Ambio*, **21**, 278–286.

Mellor, G. L., and T. Yamada, 1982: Development of a turbulence closure model for geophysical fluid problems. *Rev. Geophys.*, **20**, 851–875.

Morel, A., and S. Maritorena, 2001: Bio–optical properties of oceanic waters: A Reappraisal. *J. Geophys. Res.*, **106**, 7163–7180.

Murphy, A. H., 1992: Climatology, persistence, and their linear combination as standards of reference in skill scores. *Wea. Forecasting*, **7**, 692–698.

——, 1988: Skill scores based on the mean square error and their relationships to the correlation coefficient. *Mon. Wea. Rev.*, **116**, 2417–2424.

——, and H. Daan, 1985: Forecast evaluation. *Probability, Statistics, and Decision Making in the Atmospheric Sciences*, A. H. Murphy and R. W. Katz, Eds., Westview Press, 379–437.

Murtugudde, R., J. Beauchamp, C. R. McClain, M. R. Lewis, and A. J. Busalacchi, 2002: Effects of penetrative radiation on the upper tropical ocean circulation. *J. Climate*, **15**, 470–486.

Nakamoto, S., P. Kumar, J.–M. Oberhuber, J. Ishizaka, K. Muneyama, and R. Frouin, 2001: Response of the equatorial Pacific to chlorophyll pigment in a mixed layer isopycnal ocean general circulation model. *Geophys. Res. Lett.*, **28**, 2021–2024.

Neter, J., W. Wasserman, and G. A. Whitmore, 1988: *Applied Statistics.* Allyn and Bacon, 1006 pp.

Nihoul, J. C. J., E. Deleersnijder, and S. Djenidi, 1989: Modeling the general circulation of shelf seas by 3D

k–ϵ models. *Earth Sci. Rev.*, **26**, 163–189.

Oguz, T., P. Malanotte–Rizzoli, H. W. Ducklow, and J. W. Murray, 2002: Interdisciplinary studies integrating the Black Sea biogeochemistry and circulation dynamics. *Oceanography*, **15**, 4–11.

——, and P. Malanotte–Rizzoli, 1996: Seasonal variability of wind and thermohaline driven circulation in the Black Sea: Modeling studies. *J. Geophys. Res.*, **101**, 16 551–16 569.

——, ——, and D. Aubrey, 1995: Wind and thermohaline circulation of the Black Sea driven by yearly mean climatological forcing. *J. Geophys. Res.*, **100**, 6845–6863.

Rachev, N. H., and E. V. Stanev, 1997: Eddy processes in semi–enclosed seas. A case study for the Black Sea. *J. Phys. Oceanogr.*, **27**, 1581–1601.

Rayner, N. A., E. B. Horton, D. E. Parker, C. K. Folland, and R. B. Hackett, 1996: Version 2.2 of the Global sea–Ice and Sea Surface Temperature data set, 1903–1994. *Climate Research Tech. Note*, **74**, 42 pp. [Available from Hadley Centre, Met Office, Bracknell, UK.]

Reynolds, R. W., N. A. Rayner, T. M. Smith, and D. C. Stokes, 2002: An improved in–situ and satellite SST analysis for climate. *J. Climate*, **15**, 1609–1625.

Rochford, P. A., A. B. Kara, A. J. Wallcraft, and R. A. Arnone, 2001: Importance of solar subsurface heating in ocean general circulation models. *J. Geophys. Res.*, **106**, 30 923–30 938.

Rosmond, T. E., J. Teixeira, M. Peng, T. F. Hogan, and R. Pauley, 2002: Navy Operational Global Atmospheric Prediction System (NOGAPS): Forcing for ocean models. *Oceanography*, **15**, 99–108.

Schneider, E. K., and Z. Zhu, 1998: Sensitivity of the simulated annual cycle of sea surface temperature in the equatorial Pacific to sunlight penetration. *J. Climate*, **11**, 1933–1950.

Smith, T. M., and R. W. Reynolds, 1998: A high–resolution global sea surface temperature climatology for

the 1961–90 base period. *J. Climate*, **11**, 3320–3323.

Stanev, E. V., and J. V. Staneva, 2001: The sensitivity of the heat exchange at ocean surface to meso and sub–basin scale eddies. Model study for the Black Sea. *Dyn. Atmos. Oceans*, **33**, 163–189.

——, P. Y. Le Traon, and E. L. Peneva, 2000: Seasonal and interannual variations of sea level and their dependency on meteorological and hydrological forcing. Analysis of altimeter and surface data for the Black Sea. *J. Geophys. Res.*, **105**, 17 203–17 216.

——, and J. V. Staneva, 2000: The impact of the baroclinic eddies and basin oscillations on the transitions between different quasi–stable states of the Black Sea circulation. *J. Mar. Sys.*, **24**, 3–26.

——, and J.–M. Beckers, 1999: Numerical simulations of seasonal and interannual variability of the Black Sea thermohaline circulation. *J. Mar. Sys.*, **22**, 241–267.

——, and N. H. Rachev, 1999: Numerical study on the planetary Rossby waves in the Black Sea. *J. Mar. Sys.*, **21**, 283–306.

——, V. M. Roussenov, N. H. Rachev, and J. V. Staneva, 1995: Sea response to atmospheric variability. Model study for the Black Sea. *J. Mar. Sys.*, **6**, 241–267.

Staneva, J. V., D. E. Dietrich, E. V. Stanev, and M. J. Bowman, 2001: Rim current and coastal eddy mechanisms in an eddy–resolving Black Sea general circulation. *J. Mar. Sys.*, **31**, 137–157.

——, and E. V. Stanev, 1998: Oceanic response to atmospheric forcing derived from different climatic data sets. *Ocean. Acta*, **21**, 393–417.

Sur, H. I., E. Ozsoy, Y. P. Ilyin, and U. Unluata, 1996: Coastal/deep ocean interactions in the Black Sea and their ecological/environmental impacts. *J. Mar. Sys.*, **7**, 293–320.

——, ——, and U. Unluata, 1994: Boundary current instabilities, upwelling, shelf mixing and eutrophication

processes in the Black Sea. *Prog. Oceanogr.*, **33**, 249–302.

Vörösmarty, C. J., K. Sharma, B. M. Fekete, A. H. Copeland, J. Holden, J. Marble, and J. A. Lough, 1997: The storage and aging of continental runoff in large reservoir systems of the world. *Ambio*, **26**, 210–219.

Wallcraft, A. J., A. B. Kara, H. E. Hurlburt, and P. A. Rochford, 2003: The NRL Layered Global Ocean Model (NLOM) with an embedded mixed layer sub–model: Formulation and tuning. *J. Atmos. Oceanic Technol.*, in press

Yuen, C. W., J. Y. Cherniawsky, C. A. Lin, and L. A. Mysak, 1992: An upper ocean general circulation model for climate studies: Global simulation with seasonal cycle. *Climate Dyn.*, **7**, 1–18.

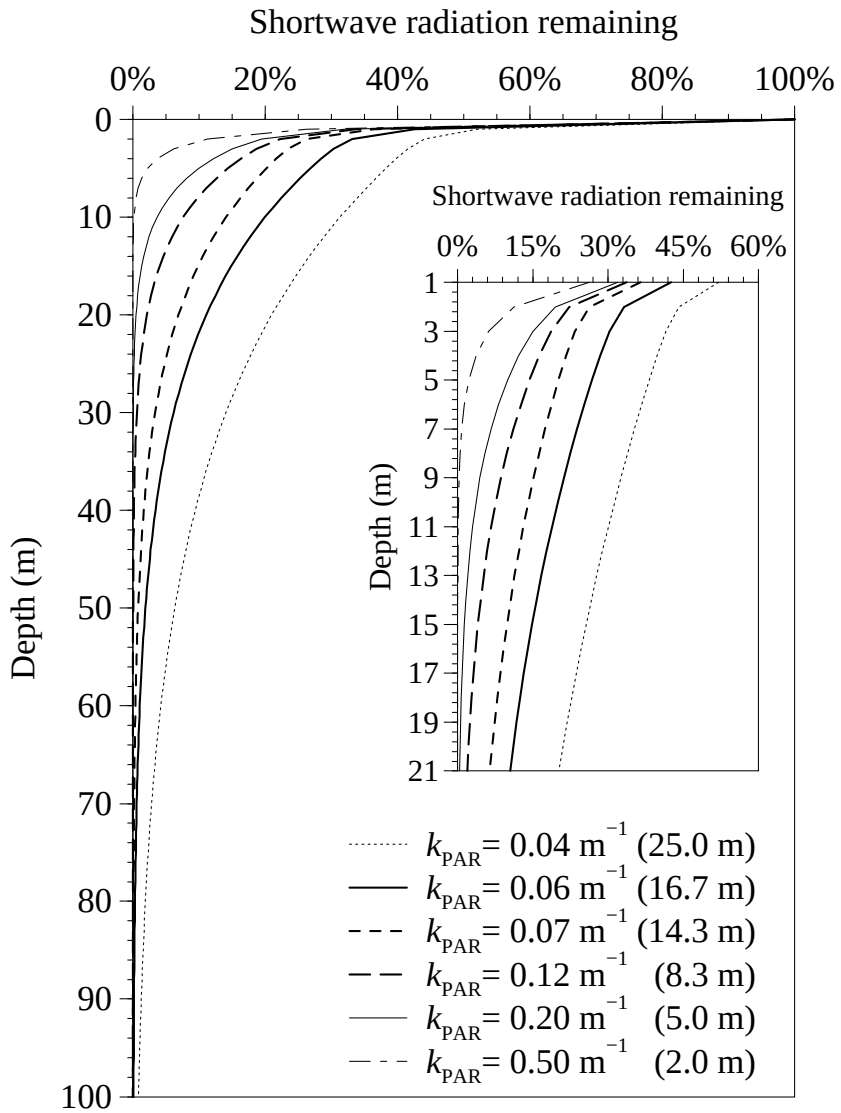

Figure 1: Percentage of penetrating shortwave radiation remaining below the sea surface vs depth used in the Black Sea HYCOM subsurface heating parameterization. The small panel inside the figure is intended to show absorption values from 1 to 21 m near the sea surface. The HYCOM k_{PAR} values of 0.04345, 0.0500, 0.0588, 0.0714, 0.1266 and 2.00 m^{-1} correspond to Jerlov I, IA, IB, II, III and mud cases, respectively. Note that HYCOM uses a 0.5 m e–folding depth for the red spectrum; thus, as k_{PAR} is greater than 0.50 m^{-1}, it matters little what fraction is in the each band because both bands have small 0.5 m e–folding depth.

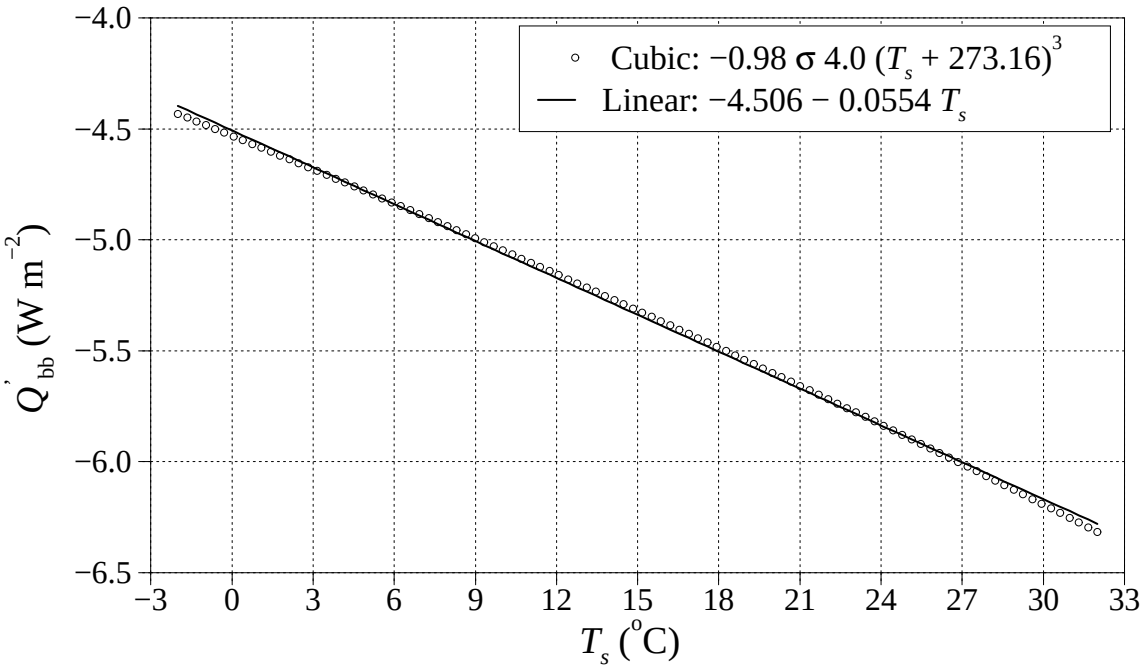

Figure 2: A linear approximation to the blackbody radiation correction based on the original cubic function. The T_s values shown on the x–axis are essentially SSTs from –2° to 32°C. The Stefan–Boltzmann constant (σ) in the cubic formulation is 5.67×10^{-8}. For simulations using interannual atmospheric forcing, the SST used to derive Q_{LW} is usually available and it can be read in as an additional "forcing" term. Note that this typically is not an accurate SST on the scales of a high resolution ocean model; thus, on the smallest scales this is a genuine and needed longwave correction. For coupled atmosphere–ocean models, the atmospheric model is presumably using the ocean SST and so the correction would be zero if they are both on the same grid. There could still be a longwave correction if the ocean model was on a finer grid than the atmospheric model.

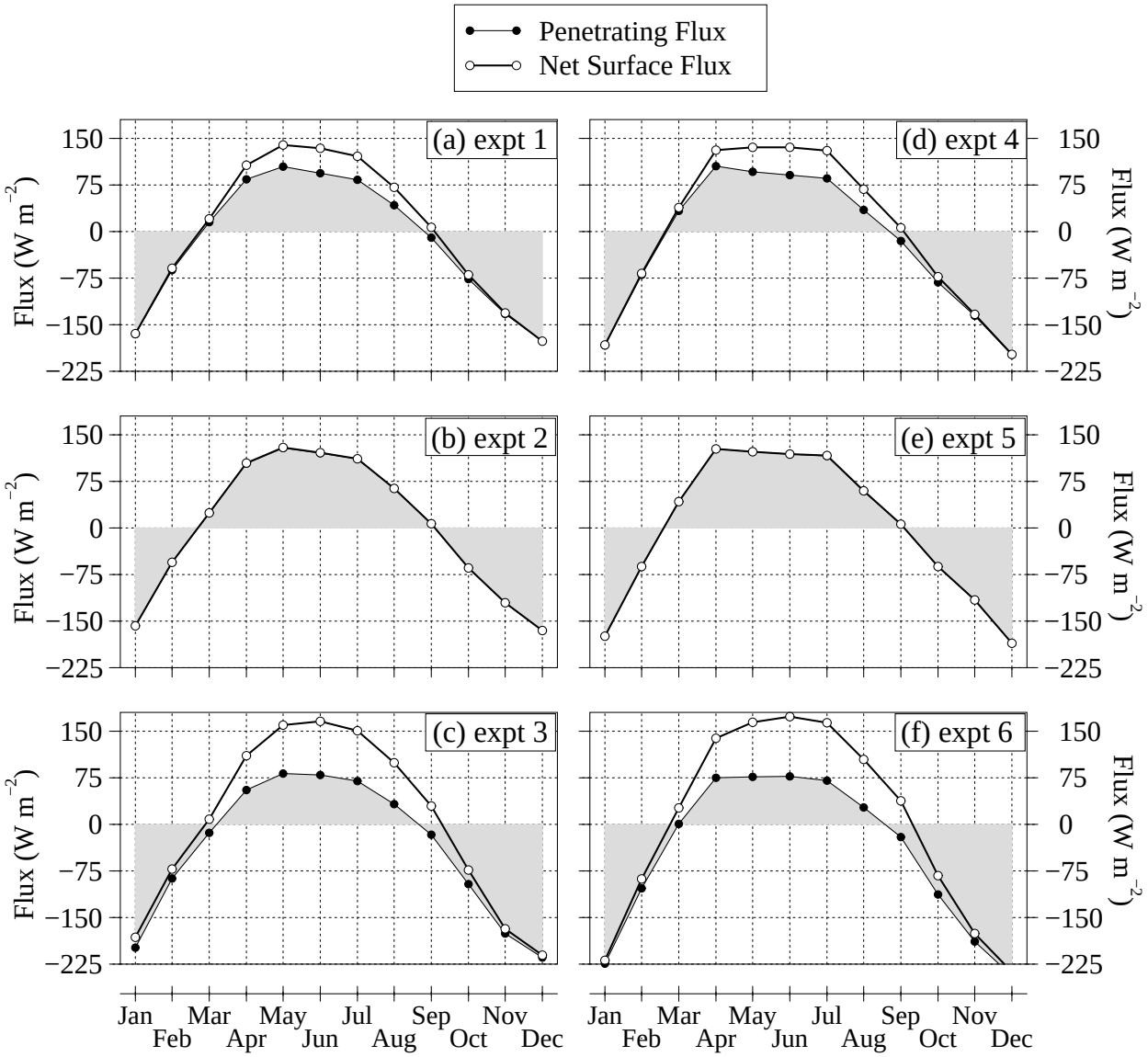

Figure 3: The basin–wide monthly mean net penetrative heat flux at the sea surface and the heat flux absorbed in the mixed layer for HYCOM simulations forced with the climatological ECMWF wind/thermal fluxes (expts 1, 2 and 3) and NOGAPS wind/thermal fluxes (expts 4,5 and 6). The difference between these two curves is the shortwave radiation absorbed below the mixed layer. The reader is referred to Table 2 for a description of each simulation. Note that monthly mean flux values were formed using daily model fluxes. The negative sign represents heat loss from the ocean.

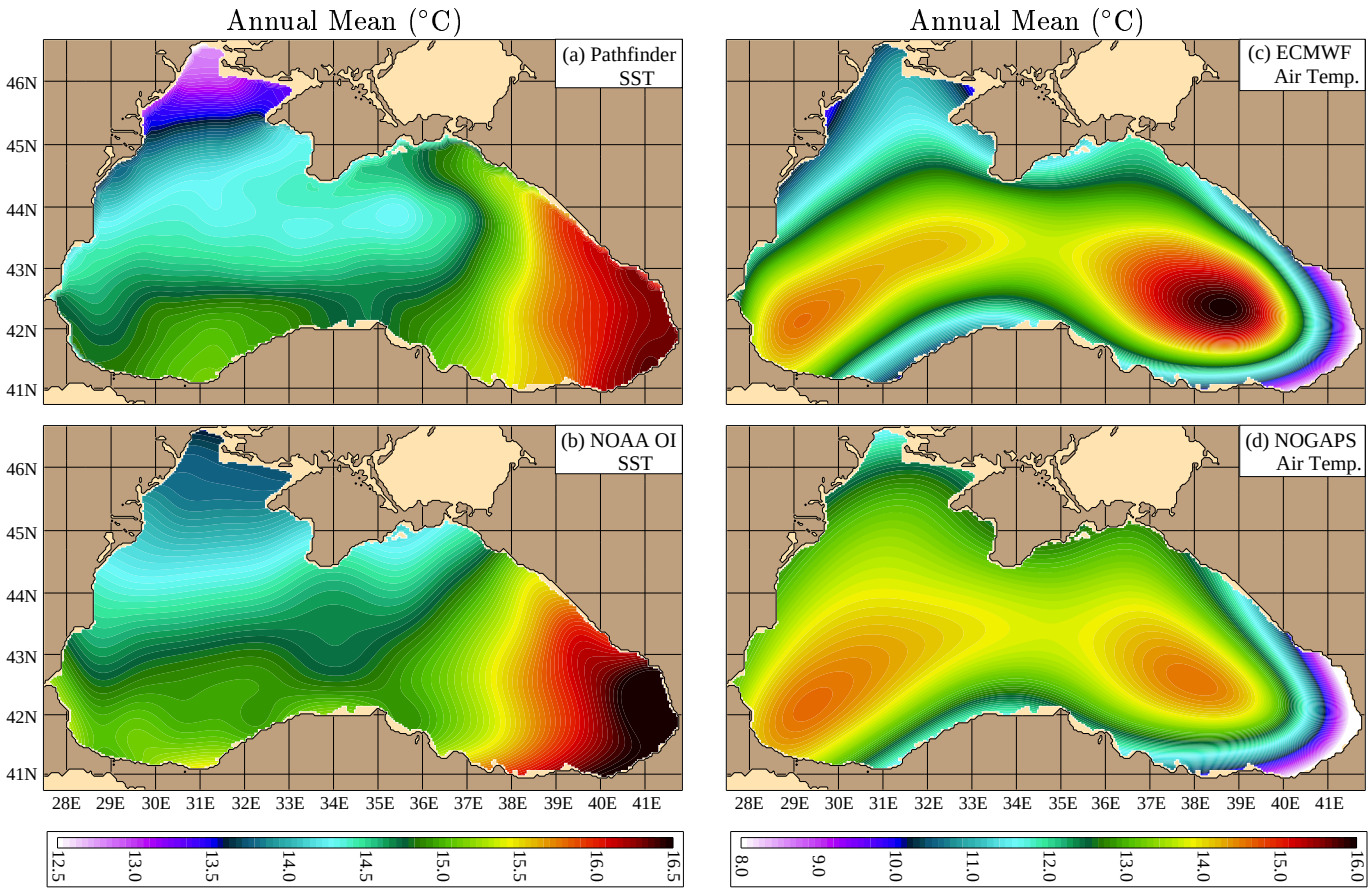

Figure 4: Climatological annual mean of sea surface temperature (SST) and air temperature at 10 m above the sea surface (T_a) over the Black Sea: (a) $1/11^\circ \times 1/8^\circ$ (longitude $\times$ latitude) Pathfinder SST climatology which can be accessed through the Earth Observing System Data and Information System (EOSDIS) Physical Oceanography Distributed Active Archive Center (PO.DAAC) at the Jet Propulsion Laboratory (JPL), (b) $1^\circ \times 1^\circ$ National Oceanic and Atmospheric Administration (NOAA) SST climatology which was developed at the Climate Prediction Center, (c) $1.125^\circ \times 1.125^\circ$ European Centre for Medium–Range Weather Forecasts (ECMWF) re–analysis T_a product, and (d) $1^\circ \times 1^\circ$ Fleet Numerical Meteorology and Oceanography Center (FNMOC) Navy Operational Global Atmospheric Prediction System (NOGAPS) T_a product. Annual means of T_a were formed during 1979–1993 for ECMWF and 1998–2002 for NOGAPS at the Naval Research Laboratory (NRL), Stennis Space Center. Note that all fields shown are interpolated to the Black Sea HYCOM domain.

(a) Annual mean SST obtained from HYCOM simulations

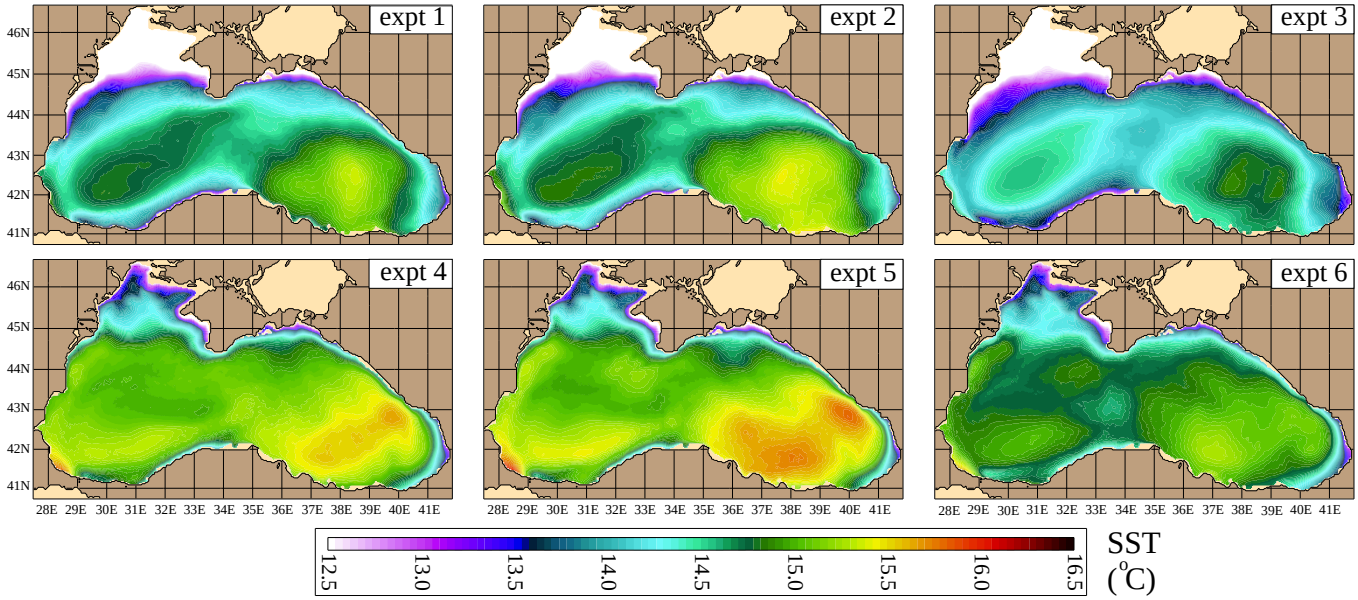

(b) SST mean error with respect to the 1/8° Pathfinder SST climatology

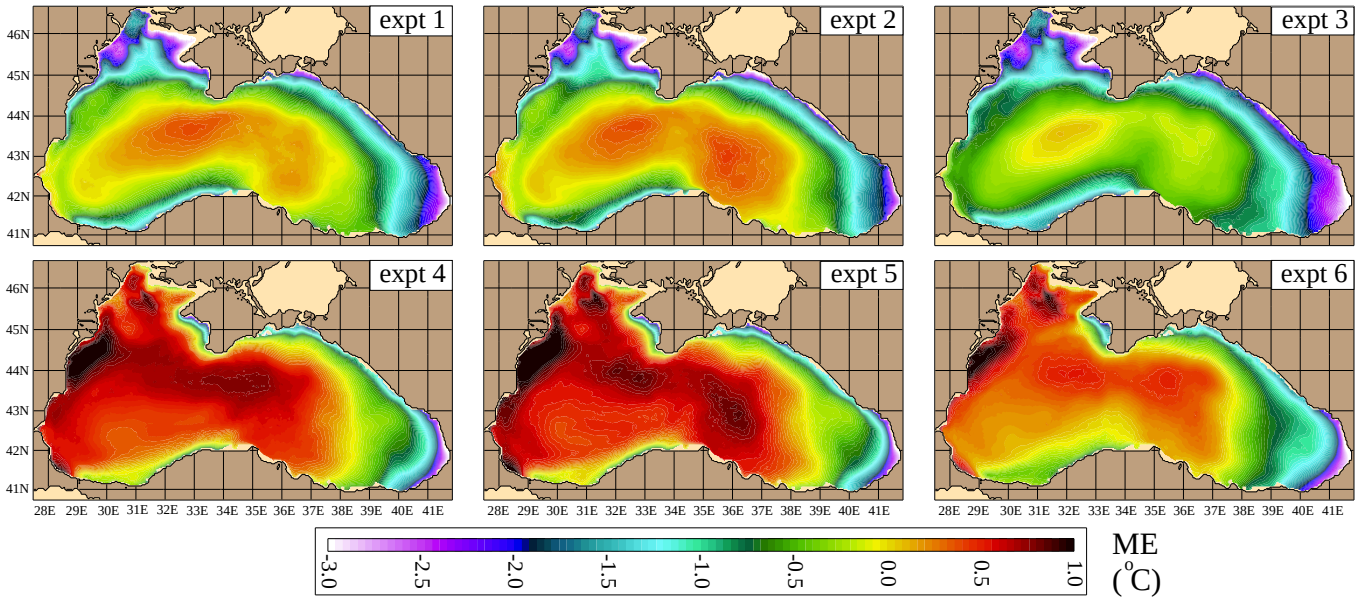

Figure 5: Model SST results: (a) Annual mean HYCOM SST, and (b) annual mean bias (i.e., ME) with respect to the satellite–based 1/8° Pathfinder SST climatology. Expts 1 and 4 represent the standard simulations which use spatial and temporal varying attenuation of Photosyntetically Available Radiation (k_{PAR}). Note that expts 1,2 and 3 are forced with ECMWF wind/thermal fluxes, and expts 4,5 and 6 are forced with NOGAPS wind/thermal fluxes. All model simulations are performed with no assimilation of any SST data.

(a) Monthly Mean SST difference in February

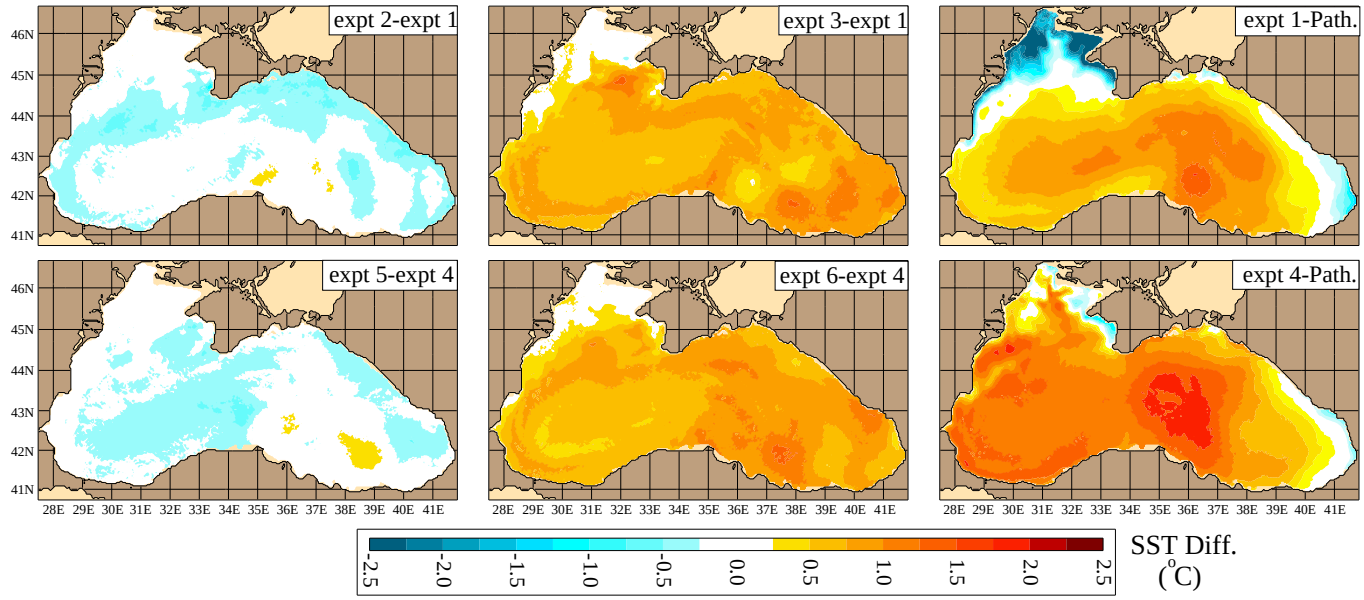

(b) Monthly Mean SST difference in June

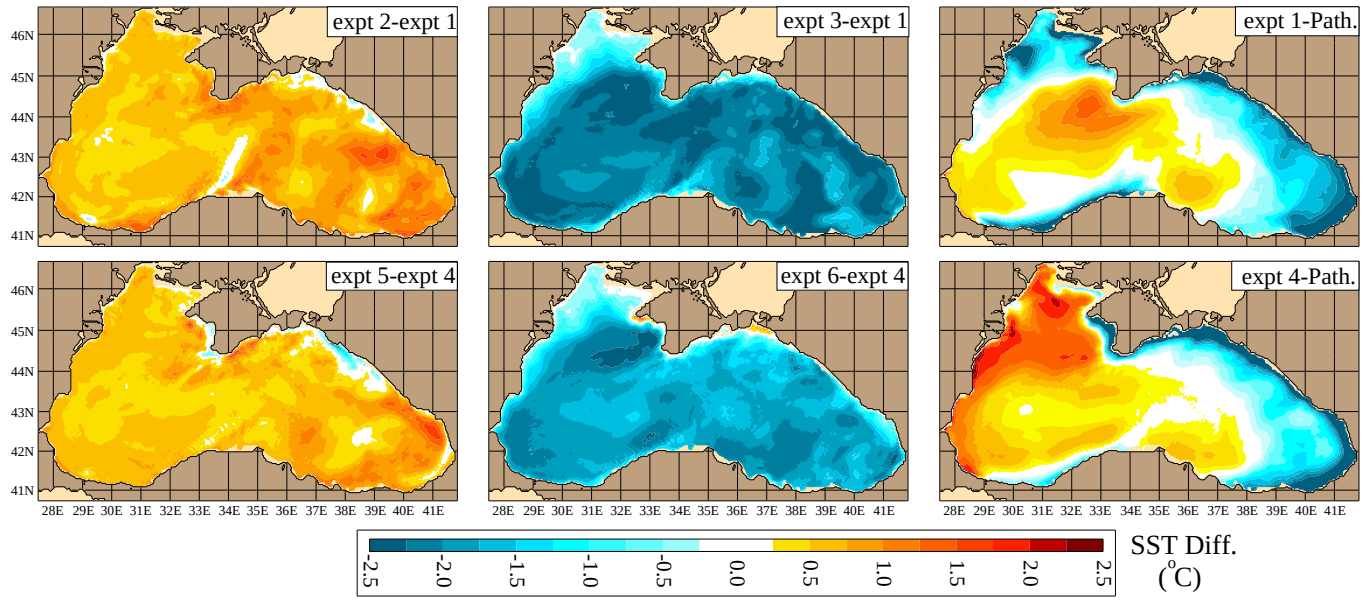

Figure 6: Mean SST difference between various experiments: (a) February, and (b) June. Expts 1 and 4 represent the standard simulations which use spatial and temporal varying attenuation of Photosyntetically Available Radiation (k_{PAR}). Note that expts 1,2 and 3 are forced with ECMWF wind/thermal fluxes, and expts 4,5 and 6 are forced with NOGAPS wind/thermal fluxes. The observed climatological SST (Clim.) is the satellite–based 1/8° Pathfinder SST climatology, and it is interpolated to the model domain to calculate differences at each grid point. All model simulations are performed with no assimilation of any SST data.

(a) SST RMS difference with respect to the 1/8° Pathfinder SST climatology

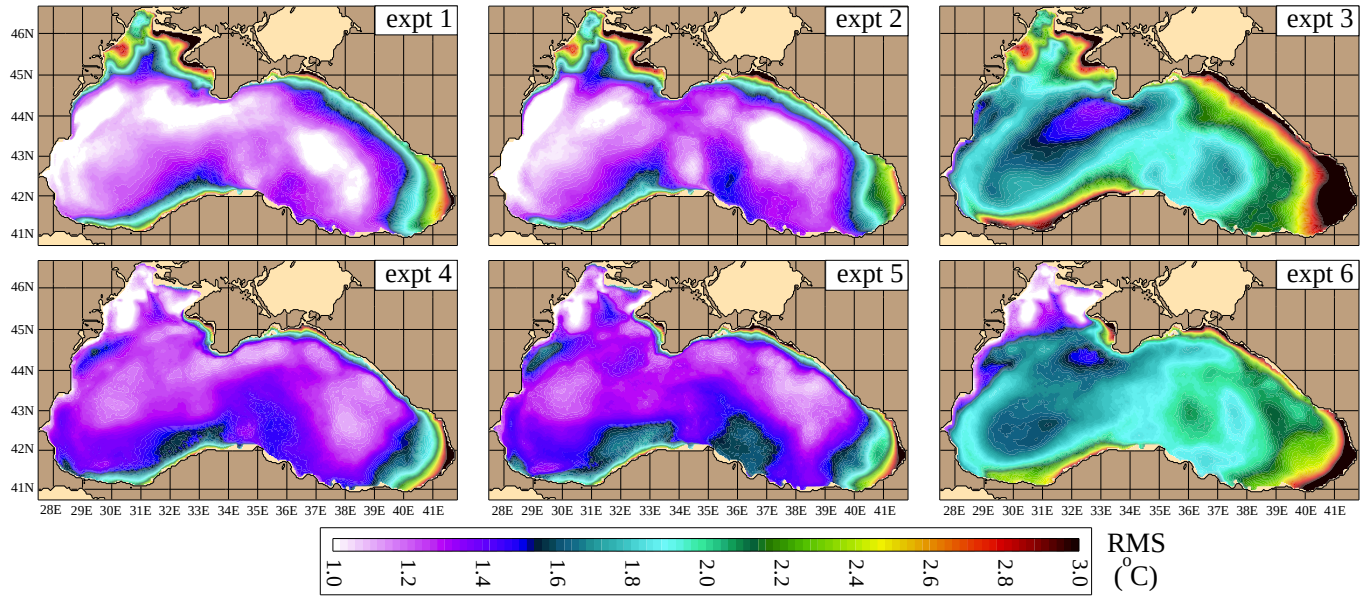

(b) SST skill score with respect to the 1/8° Pathfinder SST climatology

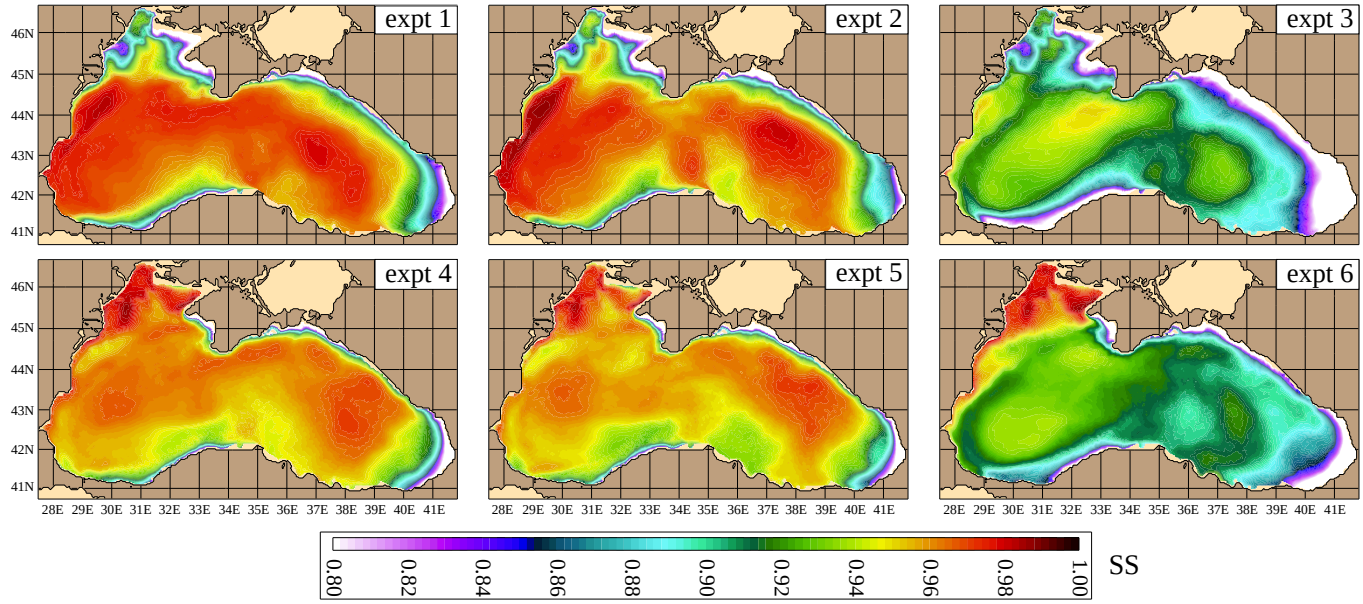

Figure 7: Statistical maps between HYCOM SST and the 1/8° Pathfinder climatology: (a) The root–mean–square (RMS) difference, and (b) skill score (SS). Note that expts 1,2 and 3 are forced with ECMWF wind/thermal fluxes, and expts 4,5 and 6 are forced with NOGAPS wind/thermal fluxes. In these comparisons the Pathfinder SST climatology is treated as "perfect", thus HYCOM can never be more accurate than the Pathfinder SST climatology. A SS value of 1.0 indicates perfect SST predictions from HYCOM. The basin averaged RMS difference and SS values are given in Table 4 for each experiment.

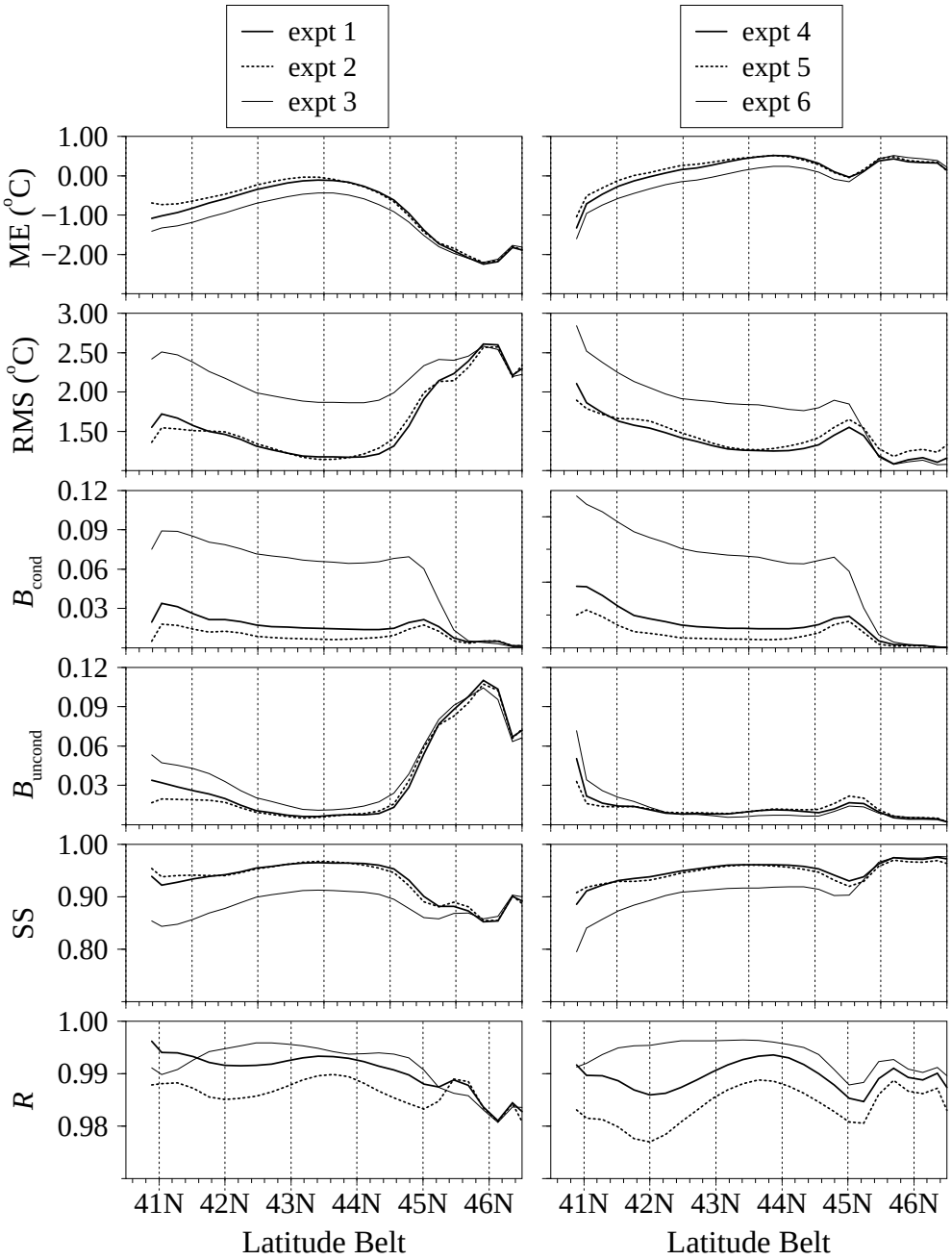

Figure 8: The zonal averages of statistical metrics calculated using monthly mean sea surface temperature (SST) between the 1/8° Pathfinder climatology and HYCOM at each model grid point over the Black Sea: From top to bottom the mean error (ME) in °C, root–mean–square (RMS) difference in °C, conditional bias (B_{cond}), unconditional bias (B_{uncond}), nondimensional skill score (SS), and correlation coefficient (R). Results are shown for expt 1 (thick solid line), expt 2 (dotted line), and expt 3 (solid) line when the model was forced with ECMWF wind/thermal fluxes; similarly expt 4 (thick solid line), expt 5 (dotted line), and expt 6 (solid) line when the model was forced with NOGAPS wind/thermal fluxes as well.

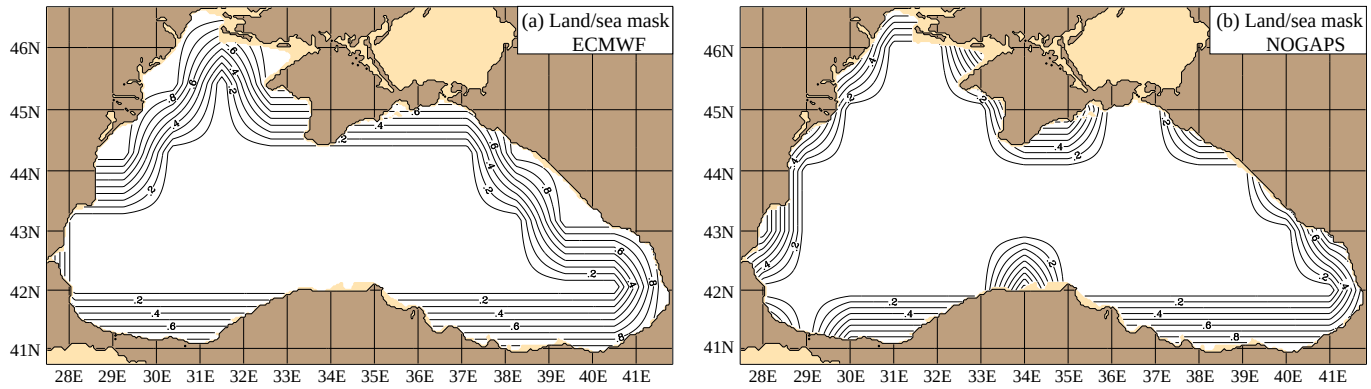

Figure 9: The land–sea mask of the Black Sea used in the (a) ECMWF re–analysis product (1979–1993), and (b) NOGAPS product (1998–2002). The original land/sea mask files are binary, i.e., a grid point is either land (1) or sea (0). We interpolated them from the $1.125^\circ \times 1.125^\circ$ reduced Gaussian grid for ECMWF and $1.0^\circ \times 1.0^\circ$ for NOGAPS to the model grid. In the figures, for example, a contour value of 0.8 implies that the flux values on the model grid were $\approx 80\%$ contaminated by the land flux values.

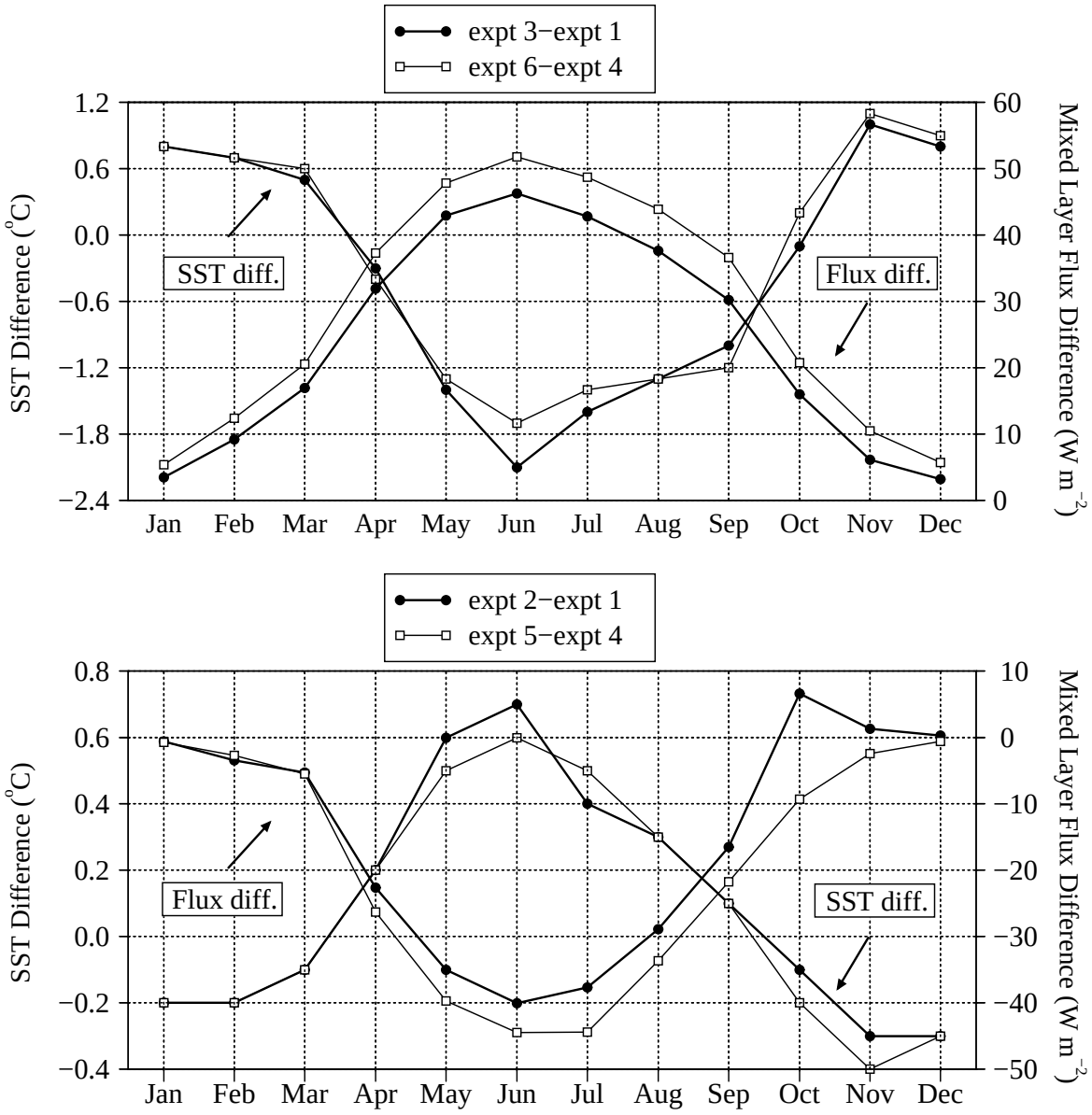

Figure 10: Monthly mean SST difference and mixed layer heat flux difference (i.e., the shortwave radiation absorbed below the mixed layer). The top panel shows differences between the clear water constant attenuation depth simulations (i.e., expts 3 and 6) and standard simulations that use spatial and temporal attenuation depths (i.e., expts 1 and 4, respectively). The bottom panel shows differences between the simulations which assume all radiation absorbed at the sea surface (expts 2 and 5) and the standard simulations. Note that the y–axis on the left includes SST differences and the one on the right includes flux differences.

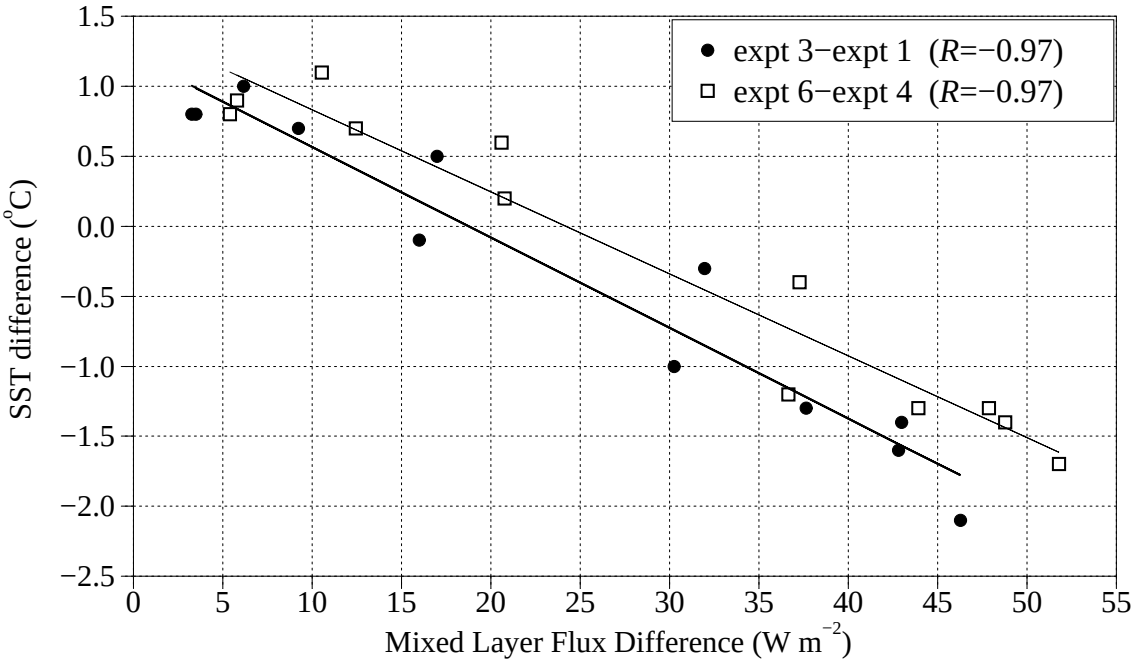

Figure 11: A scatter diagram of mixed layer flux difference vs SST differences between the simulations which use clear water constant attenuation depth (i.e., expts 3 and 6) and the standard simulations which use spatial and temporal attenuation depths (i.e., expts 1 and 4). This figure basically shows scatter plots of SST and mixed layer flux difference values whose time series are plotted in Figure 10. Also given in the figure are least squares lines for expt 3–expt 1 (dark solid line) and for expt 6–expt 4 (thin solid line). Linear correlation coefficient (R) is given on the upper right corner for each case. Slope values are –0.065 and –0.058 °C/W m^{-2} for expt 3–expt 1 and expt 6–expt 4, respectively.

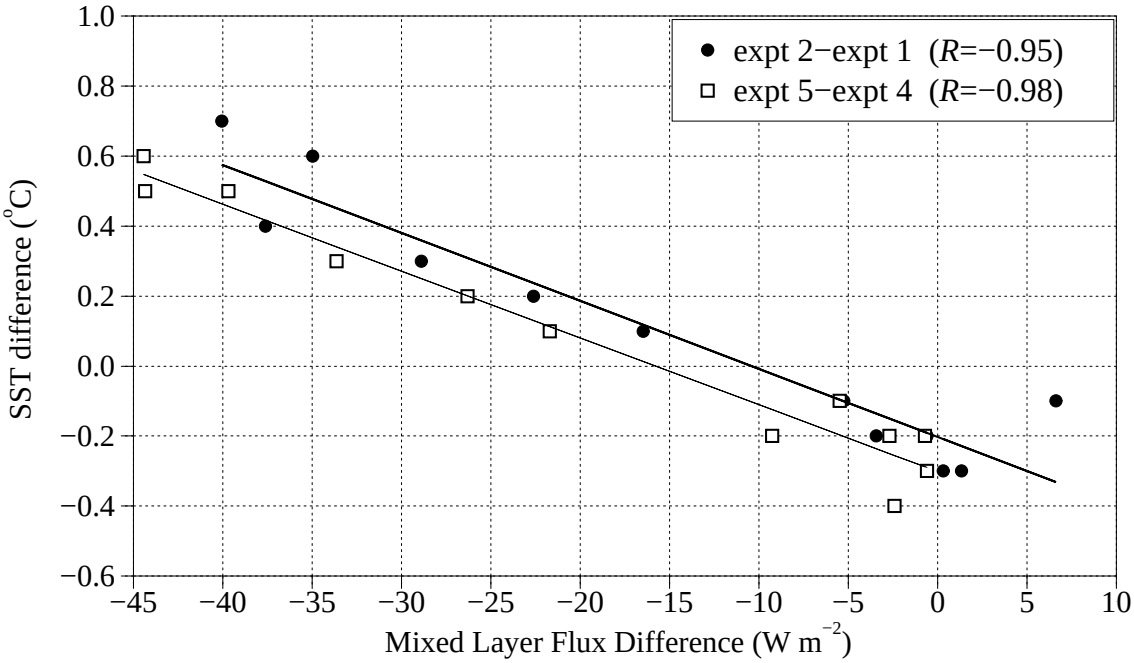

Figure 12: A scatter diagram of mixed layer flux difference vs SST differences between the simulations which assume all radiation absorbed at the sea surface (i.e., expts 2 and 5) and the standard simulations which use spatial and temporal attenuation depths (i.e., expts 1 and 4). Also given in the figure are least squares lines for expt 2–expt 1 (dark solid line) and for expt 5–expt 4 (thin solid line). Linear correlation coefficient (R) is given on the upper right corner for each case. Slope values are –0.020 and –0.019 °C/W m^{-2} for expt 3–expt 1 and expt 6–expt 4, respectively.

Table 1: Most commonly used eddy–resolving ocean models for Black Sea studies: Princeton Ocean Model (POM), Modular Ocean Model version 1 (MOM) , Dietrich Center for Air Sea Technology (DieCAST) and GeoHydrodynamics Environment Research (GHER). The numerical ocean model used in each study is also given, along with its approximate zonal and meridional grid resolutions and the number of levels in the vertical. Zonal grid spacing (lon) in km is calculated using $1^\circ \approx 111.2$ km and meridional grid spacing (lat) in km is calculated using $111.2 \times \cos(43^\circ)$ where an approximate latitude is taken as 43°.

Black Sea eddy–resolving numerical modeling studyies	Model Used	Grid resolution (lon × lat) (degrees)	(km)	Levels in Vertical
Oguz et al. (1995)	POM	$1/10^\circ \times 1/9^\circ$	11.5×08.5	18
Stanev et al. (1995)	MOM	$1/4^\circ \times 1/3^\circ$	28.0×28.0	11
Oguz and Malanotte–Rizzoli (1996)	POM	$1/10^\circ \times 1/9^\circ$	11.5×09.0	18
Rachev and Stanev (1997)	MOM	$1/10^\circ \times 1/6^\circ$	11.5×14.0	22
Staneva and Stanev (1998)	MOM	$1/4^\circ \times 1/3^\circ$	28.0×28.0	24
Stanev and Rachev (1999)	MOM	$1/10^\circ \times 1/6^\circ$	11.5×14.0	06
Stanev and Beckers (1999)	GHER	$1/7^\circ \times 1/7^\circ$	15.0×12.0	25
Stanev and Staneva (2000)	MOM	$1/12^\circ \times 1/9^\circ$	09.0×09.0	24
Kourafalou and Stanev (2001)	POM	$1/12^\circ \times 1/9^\circ$	09.0×09.0	16
Stanev and Staneva (2001)	MOM	$1/12^\circ \times 1/9^\circ$	09.0×09.0	24
Staneva et al. (2001)	DieCAST	$1/12^\circ \times 1/9^\circ$	09.0×09.0	20
This study	HYCOM	$1/25^\circ \times 1/32^\circ$	03.2×03.2	15

Table 2: The six HYCOM simulations performed. The wind and thermal forcing (i.e., air temperature at 10 m, air mixing ratio at 10 m, shortwave and longwave radiation) are from the 6–hourly European Centre for Medium Range Weather Forecasts (ECMWF) and Fleet Numerical Meteorology and Oceanography Center (FNMOC) Navy Operational Global Atmospheric Prediction System (NOGAPS).

Expt.	k_{PAR}	Description of the experiment	Forcing
expt 1	Variable	Spatial and temporal attenuation depths	ECMWF
expt 2	99 m^{-1}	All solar radiation absorbed at the surface	ECMWF
expt 3	0.06 m^{-1}	Constant attenuation depth in the Black Sea	ECMWF
expt 4	Variable	Spatial and temporal attenuation depths	NOGAPS
expt 5	99 m^{-1}	All solar radiation absorbed at the surface	NOGAPS
expt 6	0.06 m^{-1}	Constant attenuation depth in the Black Sea	NOGAPS

Table 3: Basin averaged monthly mean SST differences between various experiments (see Table 2 for a description of each simulation). Also given are the basin averaged SST differences between the standard simulations (i.e., expts 1 and 4) and the 1/8° climatological Pathfinder SST (Clim.) as described in the text. Coldest and warmest SST differences that are seen over the Black Sea are also written to show how cold/warm these differences can be.

SST Difference	Jan	Feb	Mar	Apr	May	Jun	Jul	Aug	Sep	Oct	Nov	Dec
Mean (°C)												
expt 2–expt 1	-0.2	-0.2	-0.1	0.2	0.6	0.7	0.4	0.3	0.1	-0.1	-0.3	-0.3
expt 3–expt 1	0.8	0.7	0.5	-0.3	-1.4	-2.1	-1.6	-1.3	-1.0	-0.1	1.0	0.8
expt 1–Clim.	0.5	0.6	0.2	0.3	0.4	-0.4	-1.6	-2.1	-1.8	-1.8	-1.2	0.3
expt 5–expt 4	-0.2	-0.2	-0.1	0.2	0.5	0.6	0.5	0.3	0.1	-0.2	-0.4	-0.3
expt 6–expt 4	0.8	0.7	0.6	-0.4	-1.3	-1.7	-1.4	-1.3	-1.2	0.2	1.1	0.9
expt 4–Clim.	1.0	1.2	0.9	1.8	1.6	0.1	-0.7	-1.4	-1.1	-1.3	-0.6	0.8
Minimum (°C)												
expt 2–expt 1	-0.8	-1.2	-1.4	-0.5	-0.6	-0.8	-2.4	-2.1	-1.0	-1.0	-1.1	-0.9
expt 3–expt 1	-0.3	-0.3	-0.4	-0.8	-2.3	-2.9	-2.7	-2.9	-2.1	-1.8	-0.1	-0.1
expt 1–Clim.	-1.5	-1.0	-1.6	-1.9	-1.6	-1.8	-2.6	-2.4	-1.9	-1.5	-1.3	-0.8
expt 5–expt 4	-0.9	-0.7	-0.5	-0.5	-1.2	-2.6	-1.8	-2.5	-0.9	-1.0	-1.3	-0.9
expt 6–expt 4	-0.1	-0.2	-0.3	-1.0	-2.2	-3.0	-2.6	-2.6	-2.0	-0.8	0.1	-0.1
expt 4–Clim.	-1.2	-1.2	-1.1	-0.5	-1.1	-2.9	-2.3	-2.5	-1.7	-1.9	-1.7	-1.6
Maximum (°C)												
expt 2–expt 1	0.6	0.4	0.5	0.9	1.5	1.7	1.4	1.7	1.1	0.8	0.4	0.3
expt 3–expt 1	1.3	1.4	1.1	0.7	0.3	0.3	0.9	1.7	1.6	2.3	1.7	1.4
expt 1–Clim.	1.9	1.8	1.3	1.6	2.3	2.3	1.4	-0.1	-0.2	0.7	1.4	2.1
expt 5–expt 4	0.5	0.4	0.3	0.9	1.3	1.8	1.9	1.4	0.8	0.3	0.4	0.4
expt 6–expt 4	1.5	1.4	0.9	0.5	0.7	2.3	2.9	1.8	1.3	1.5	2.1	1.7
expt 4–Clim.	2.1	2.0	1.9	3.0	3.2	3.2	1.4	0.6	1.7	2.2	1.9	2.7

Table 4: Basin averaged SST validation statistics for the six HYCOM simulations performed. Reader is referred to section 4a for a detailed description of statistical measures. Statistics are calculated using monthly mean values. All R values are greater than 0.97 and statistically significant in comparison to a 0.7 correlation value at 95% confidence interval. Note that a correlation coefficient of 0.98 is not statistically different from a correlation coefficient of 0.99.

	ME (°C)	RMS (°C)	B_{cond}	B_{uncond}	SS	R
expt 1	-0.54	1.41	0.017	0.020	0.95	0.99
expt 2	-0.49	1.41	0.010	0.018	0.95	0.99
expt 3	-0.85	2.06	0.068	0.028	0.89	0.99
expt 4	0.19	1.39	0.019	0.011	0.95	0.99
expt 5	0.25	1.45	0.010	0.011	0.95	0.98
expt 6	-0.07	1.89	0.071	0.010	0.91	0.99